THE ENERGY SPECTRA OF URANIUM ATOMS SPUTTERED FROM URANIUM METAL AND URANIUM DIOXIDE TARGETS

Thesis by

Robert Allen Weller, Jr.

In Partial Fulfillment of the Requirements

for the Degree of

Doctor of Philosophy

California Institute of Technology

Pasadena, California

1978

(Submitted March 6, 1978)

Acknowledgments

I am especially grateful to Professor Tom Tombrello for accepting me as a student. His suggestions and encouragement have been decisive factors in this work. I would also like to thank Professor D. S. Burnett for the unrestricted use of his laboratory facilities and for many helpful discussions.

I have benefitted from conversations with many persons while engaged in this project. I would like to mention especially, Professor C. Barnes, B. Cooper, C. Filleux, R. Gregg, J. Griffith, Professor P. Haff, Professor S. Koonin, W. Russell and Z. Switkowski.

The highly competent technical and secretarial staffs of the Kellogg Laboratory have played an essential part in this work. I wish, in particular, to thank Mr. W. Schick.

Finally, I wish to acknowledge the love and support of my family, my wife Mari, my mother Elizabeth, my sister Elaine, and, of course, my Aunt Minnie Belle. Here too I must mention my Dad. Although he is gone, his influence still touches me and my work.

This research project has been supported in part by the National Science Foundation, the National Aeronautics and Space Administration, the Department of Energy and the Ford Motor Company.

Abstract

The energy spectra of ^{235}U atoms sputtered from a 93% enriched ^{235}U metal foil and a hot pressed $^{235}UO_2$ pellet by an 80 keV $^{40}Ar^+$ beam have been measured in the range 1 eV to 1 keV. The measurements were made using a mechanical time-of-flight spectrometer in conjunction with the fission track technique for detecting ^{235}U. The design and construction of this spectrometer are discussed in detail, and its operation is mathematically analyzed.

The results of the experiment are discussed in the context of the random collision cascade model of sputtering. The spectrum obtained by the sputtering of the ^{235}U metal target was found to be well described by the functional form $E(E+E_b)^{-2.77}$, where E_b = 5.4 eV. The $^{235}UO_2$ target produced a spectrum that peaked at a lower energy ($\sim$ 2 eV) and decreased somewhat more rapidly for $E \gtrsim 100$ eV.

Table of Contents

I. INTRODUCTION

When a high velocity ion or atom strikes the surface of a solid target, the collision may result in the ejection of atoms or clusters of atoms from the target material. At the macroscopic level, this process, known as sputtering, may be characterized by a generalized sputtering yield $S_i(E,\theta,\cdots;\cdots)$. Here i, an index, denotes the particular sputtered object of interest, E the energy of the sputtered object, and θ the direction of ejection with respect to the target normal. The ellipses before and after the semicolon indicate that from time to time other continuous or discrete variables may be of interest. When $S_i(E,\theta,\cdots;\cdots)$ is integrated or summed over all variables before the semicolon (with weighting factors where necessary) the result is the total number of objects i that are ejected from the target per incident ion that strikes the surface. This quantity is called the sputtering yield. The ellipsis after the semicolon denotes initial conditions which may affect S_i, such as the ion beam energy or angle of incidence with respect to the target normal.

We shall be concerned here with the measurement of the energy spectrum, S(E), of ^{235}U atoms ejected from enriched uranium metal and uranium oxide targets (E is the ejection energy). If $S_i(E,\theta,\cdots;\cdots)$ is known--which it usually is not--then S(E) may be obtained by fixing some of the variables of S_i before the semicolon and integrating (or summing) over the others. This must, of course, be done in a way that is appropriate to the particular experimental arrangement. The parameters after the semicolon, which also affect S(E), are suppressed for economy of notation.

As McCracken (1975) has pointed out, the total sputtering yield has proved to be rather insensitive to the details of particular models of the sputtering process. Measurements of the energy distribution of the sputtered particles taken under various conditions have, therefore, been undertaken in the hope that these additional data will be more sensitive. Such measurements are difficult for two reasons: First, most of the ejected particles are neutral; second, they are quite low in energy, the most probable energy of ejection usually being between 1 eV and 10 eV. As a result, the experiments performed to date have been limited in the choices of either targets or bombardment conditions. In one common type of experiment, the post-ejection ionization of the sputtered atoms is followed by analysis. Typical of this class of experiments are those of Stuart and Wehner (1964) and Stuart et al. (1969). These experiments, which were carried out in a plasma, involved the observation of photons emitted from sputtered particles in a time-of-flight scheme. In the second experiment doppler shift measurements of the photons were also made. In another variation on this procedure, Oechsner and Reichert (1966) combined post-ionization and retarding field analysis, and later Bernhardt et al. (1976) used mass spectrometry as well. A second general class of experiments involves a time-of-flight technique to disperse the sputtered material on a collector. This collector is then analyzed by a sensitive technique to measure the quantity of deposited material. The most extensive set of sputtering measurements to date is of this type and is described by Thompson (1968), Farmery and Thompson (1968), Chapman et al. (1972), and Reid et al. (1976). All these

experiments were carried out with an apparatus first described by Thompson et al. (1968). To date only copper and gold targets have been investigated by this method with gold being the more extensively studied. In these experiments radioactive targets were sputtered by ions with energy $\geq$ 10 keV and collected material measured by autoradiography. The experiments described here are quite similar in form to these; however, time-of-flight or velocity selection experiments may differ in detail as evidenced by previous work described in the literature; e.g., Beuscher and Kopitzki (1965), Hulpke and Schlier (1967), and Politiek and Kistemaker (1969).

There were two principal reasons for undertaking this work. The first was to provide additional data for testing theoretical models of the sputtering process. The amount of energy-spectrum data is relatively small when compared to the total amount of data on other aspects of the sputtering process. This is particularly true for the sputtering of compounds and alloys. Miyagawa (1973) and Können (1974) report measurements of the energy spectrum of one or both components of a sputtered alkali halide and are typical of existing data. The technique to be described here can be applied to the sputtering of uranium compounds as easily as it can be applied to the sputtering of uranium metal. One must, however, remain constantly aware that the technique does not separate the contributions to the total energy spectrum of various sputtered molecules containing ^{235}U. In the language of the first paragraph, molecular state is a discrete variable over which a summation is done.

The second motivation for undertaking this work came from the field of planetary science. Haff et al. (1977) have shown that the

sputtering of the lunar surface by the solar wind may lead to modification of the chemical and isotopic composition of the surfaces of lunar dust grains. To see how this may occur, consider the following simple probabilistic argument. Suppose that a particle (atom) is observed to be sputtered from the lunar surface. Then one can assign probabilities to the following outcomes:

A ≡ the particle that is sputtered is of type A with mass M_A

B ≡ the particle that is sputtered is of type B with mass M_B

C ≡ the particle that is sputtered escapes the moon's gravity

Let P(A), P(B), and P(C) be the a priori probabilities of each outcome and P(A|C), P(B|C), P(C|A), and P(C|B) be various conditional probabilities. (The notation P(A|B) should be read "The probability of A given that B occurs.") These quantities are related by Bayes' theorem (Mathews and Walker 1970):

$$\frac{P(A|C)}{P(B|C)} = \frac{P(A)}{P(B)} \frac{P(C|A)}{P(C|B)} \tag{1}$$

The result of Haff et al. (1977) may be obtained from Eq. (1) by making the following three assumptions:

Assumption 1: If χ_A and χ_B are the abundances of particles A and B at the grain surface, then

$$P(A) = \chi_A \quad \text{and} \quad P(B) = \chi_B \tag{2}$$

Assumption 2: Every sputtered atom, regardless of its mass, has the same energy distribution. Let the probability of a sputtered particle having energy between E and E+dE be S(E)dE and the escape energies of

particles A and B be E_A and E_B, respectively. Then

$$P(C|A) = \int_{E_A}^{\infty} S(E)\,dE \qquad \text{and} \qquad P(C|B) = \int_{E_B}^{\infty} S(E)dE \quad . \tag{3}$$

Assumption 3: Let n_A and n_B be the abundances of A and B in the bulk of the grain. Then a condition of secular equilibrium is established in which particles enter (from the bulk) and leave the surface layer (where the abundances are χ_A and χ_B) at the same rate. That is,

$$\frac{P(A|C)}{P(B|C)} = \frac{n_A}{n_B} \tag{4}$$

Combining equations (1), (2), (3), and (4) gives

$$\frac{\chi_A}{\chi_B} = \left(\frac{n_A}{n_B}\right) \frac{\int_{E_B}^{\infty} S(E)dE}{\int_{E_A}^{\infty} S(E)\,dE} \quad . \tag{5}$$

Thus, in order to make predictions of the degree of modification of the grain surfaces, it is necessary to know the energy distribution of the sputtered atoms. While most data taken to date agree rather well with model predictions, there are some systematic deviations. Furthermore, no proven means is available for predicting the energy distributions of the various component atoms sputtered from a heterogeneous target. For this case more experimental data are clearly needed.

In Section II of this thesis an intuitive picture of the sputtering process will be presented along with the energy spectrum predictions

of accepted theories of sputtering. Sections III and IV are devoted to discussions of the experimental apparatus and experimental procedure. Finally, Section V contains the results of the measurements and a discussion.

II. THEORY

The model that best describes sputtering under the conditions prevailing in this experiment is the random collision cascade model proposed by Thompson (1968). The general features of Thompson's model were confirmed by Robinson (1965) in a more rigorous calculation. More recently, Sigmund (1972b) has discussed the energy spectrum of sputtered particles in light of other developments in the field of radiation damage. Again, the calculations confirm the dominant features of the Thompson model when all initial assumptions are the same.

The calculation presented here is similar to both Robinson's and Sigmund's work. The basic equation used is very similar to the one derived by Robinson; however, unlike Robinson's equation, this one describes the density of moving atoms rather than the collision density. In this respect it resembles Sigmund's expressions. It should be stressed that the purpose of the following is to show how simple assumptions lead to a reasonably accurate prediction of the shape of the measured energy spectrum. The result obtained will be compared with Sigmund's result which was derived more rigorously and from more realistic assumptions.

Let $p(E,t)dE$ be the number of target atoms per unit volume with energy in the interval $(E,E+dE)$ at time t. Then at a time dt later $p(E,t+dt)$ will have two parts. The first will consist of all those atoms with energy E at time t that did not suffer a collision during dt. The second will be composed of all of the atoms that were added during dt because of collisions. This second group may be further divided into

two subsets. The first subset consists of atoms that were at rest at time t and were promoted to energy E during dt by collisions. The second subset contains atoms that had some higher energy E' and lost E'-E during dt. It will be assumed throughout the following discussion that moving atoms only collide with atoms that are at rest. Then we may write

$$p(E,t+dt) = p(E,t)(1 - g(E)dt) + \int_0^\infty p(E',t)dE'\, g(E')dt\, K(E',E) \tag{6}$$

where $g(E) = N\sigma\sqrt{\frac{2}{m}}\sqrt{E} \equiv k\sqrt{E} = N\sigma v$

N = number density of stationary target atoms

m = mass of a target atom

v = velocity of atom of energy E

Let $\frac{d\sigma(E',E)}{dE}$ = differential cross section for a particle of energy E' to transfer energy E in a collision

so that $$\sigma = \int_0^{E'} \frac{d\sigma(E',E)}{dE}\, dE \quad .$$

Then the quantity K(E',E) is defined as follows:

$$K(E',E) = [\sigma(E',E) + \sigma(E',E'-E)]\, H(E'-E)\, H(T-E') \quad .$$

Here $\sigma(E',E)$ is a normalized differential cross section defined by

$$\sigma(E',E) = \frac{\frac{d\sigma(E',E)}{dE}}{\int_0^{E'} \frac{d\sigma(E',E)}{dE}\, dE}$$

and H(x) is the unit step function

$$H(x) = \begin{cases} 0 & x < 0 \\ 1 & x > 0 \end{cases} .$$

T is the maximum energy of any atom in the collision cascade.

Equation (6) can be expanded to first order in dt with the result that

$$\frac{\partial p(E,t)}{\partial t} + g(E)\, p(E,t) = \int_0^\infty p(E',t)\, K(E',E)\, g(E')dE' \quad . \qquad (7)$$

Since this equation is linear in t, it can be easily reduced to an integral equation. The result is

$$p(E,t) = e^{-g(E)t}\left[p(E,0) + \int_0^t dt'\, e^{g(E)t'} \int_0^\infty p(E',t')K(E',E)g(E')dE'\right] . \qquad (8)$$

This equation assumes that no source of moving atoms is present in the time interval (0,t). For this reason equation (8), in effect, describes the development of an "average" collision cascade. In an actual experiment, however, collisions between beam particles and target atoms provide a source of moving target atoms that may be both time and energy dependent. Let $\phi(E,t)$ be the number of target atoms set in motion in the energy interval (E,E+dE) during the time interval (t,t+dt). The effect of this source on equation (7) is to add $\phi(E,t)$ to the right side, giving

$$\frac{\partial p(E,t)}{\partial t} + g(E)\, p(E,t) = \phi(E,t) + \int_0^\infty p(E',t)K(E',E)\, g(E')dE' \quad . \qquad (9)$$

The analog of equation (8) then becomes

$$p(E,t) = e^{-g(E)t}\left[p(E,0) + \int_0^t e^{g(E)t'}\,\phi(E,t')dt' + \int_0^t dt'\, e^{g(E)t'} \int_0^\infty p(E',t')\,K(E',E)\,g(E')\,dE'\right] . \qquad (10)$$

Usually in sputtering experiments the source term $\phi(E,t)$ may be assumed to be time independent. This will result in the establishment (after an initial transient period) of a steady state $p(E,t)$ which will be denoted by $p(E)$. From either equation (10) with $t \to \infty$ or equation (9) with $\partial p(E,t)/\partial t = 0$, it is seen that $p(E)$ satisfies

$$g(E)\,p(E) = \phi(E) + \int_0^\infty p(E')\,K(E',E)\,g(E')dE' \quad . \qquad (11)$$

Thus far no assumption has been made about the differential cross section to be used in deriving $K(E',E)$ except that it leads to a finite total cross section. The simplest assumption, and the one that shall be made here, is that the target atoms behave like hard spheres in collisions with each other. In this case, $\sigma(E',E)$ is independent of E and is given by

$$\sigma(E',E) = 1/E' \quad . \qquad (12)$$

Robinson (1965) has discussed this assumption in the context of collision densities and finds that the final result is surprisingly insensitive to the exact cross section used. In addition, equation (9) may, in principle, be solved analytically when one assumes equation (12). The

steady state case (equation (11)) which is of greatest interest in a discussion of energy spectra will be solved below. The general solution of equation (9) will be presented in Appendix A.

With the assumption given in equation (12) the equation for K(E',E) becomes

$$K(E',E) = \frac{2}{E'} H(E'-E)\, H(T-E')$$

and equation (11) becomes

$$k\sqrt{E}\, p(E) = \phi(E) + \int_0^\infty p(E')\, \frac{2}{E'} H(E'-E)\, H(T-E')\, k\sqrt{E'}\, dE' \qquad (13)$$

where k was defined following equation (6). Note that the variable E appears in the integral in equation (13) only as a parameter in the term H(E'-E). Since

$$\frac{d}{dx} H(x) = \delta(x) = \text{Dirac } \delta \text{ function} \quad , \qquad (14)$$

we differentiate equation (13) to obtain

$$\frac{d}{dE}\left(k\sqrt{E}\, p(E)\right) = k\sqrt{E}\, \frac{dp(E)}{dE} + \frac{1}{2} kE^{-1/2}\, p(E) =$$

$$= \frac{d\phi(E)}{dE} - 2k \int_0^\infty p(E')\, \delta(E'-E)\, H(T-E')\, \frac{dE'}{\sqrt{E'}} \quad .$$

Because of the Dirac δ function in the integrand, the integral is trivial, and after some rearrangement we have

$$\frac{dp(E)}{dE} + \frac{1}{2} \frac{p(E)}{E} + \frac{2p(E)}{E} H(T-E) = \frac{1}{k\sqrt{E}} \frac{d\phi(E)}{dE} \quad . \qquad (15)$$

To solve this equation we must examine the two regions $E < T$ and $E > T$ separately. Consider first the region $E < T$. Then $T - E > 0$, so $H(T-E) = 1$ and equation (15) is

$$\frac{dp(E)}{dE} + \frac{5}{2}\frac{p(E)}{E} = \frac{1}{k\sqrt{E}}\frac{d\phi(E)}{dE} \quad . \tag{16}$$

This equation has the solution

$$E^{5/2}\, p(E) = \frac{1}{k}\int_0^E E'^2\, \frac{d\phi(E')}{dE'}\, dE' + C$$

where C is an arbitrary integration constant. Integration of the right side once by parts and division of the equation by $E^{5/2}$ gives finally,

$$p(E) = \frac{\phi(E)}{k\sqrt{E}} - \frac{2}{kE^{5/2}}\int_0^E E'\, \phi(E')\, dE' + CE^{-5/2} \tag{17}$$

In order to fix the value of C, note from equation (13) that

$$\lim_{E \to T} p(E) = \frac{\phi(T)}{k\sqrt{T}} \quad . \tag{18}$$

As a result

$$C = \frac{2}{k}\int_0^T E'\, \phi(E')dE'$$

and finally,

$$p(E) = \frac{2}{kE^{5/2}}\int_0^T E'\, \phi(E')dE' + \frac{\phi(E)}{kE^{1/2}} - \frac{2}{kE^{5/2}}\int_0^E E'\, \phi(E')\, dE' \quad . \tag{19}$$

In the second region, $E \to T$, both $\phi(E)$ and $p(E)$ are equal to zero.

Before proceeding with equation (19) it is necessary to make some assumptions. First, however, note that if the source of moving target atoms is a beam of particles of energy E_o, then the value of $\phi(E)$ is

$$\phi(E) = N\Phi \frac{d\bar{\sigma}(E_o,E)}{dE} \tag{20}$$

where N is the density of target atoms, Φ the flux of beam particles, and $d\bar{\sigma}(E_o,E)/dE$ is the differential cross section for transfer of energy E to a target atom by a beam atom. Although it is not particularly crucial, we will assume that this cross section is the one used by Lindhard *et al.* (1963) in their work on particle ranges and stopping powers. For the case of argon atoms bombarding a uranium target, as in this experiment, the function $\phi(E)$ increases monotonically in the range $E < T$. Since we will be interested only in the region $E \ll T$, the first approximation will be to neglect the last term on the right side of equation (19) because it is clearly much smaller than the first. The middle term on the right of equation (19) is a contribution to p(E) that results directly from collisions of the incident beam. Numerically, it is much smaller than the first. Furthermore, it is kinematically impossible for direct recoils to contribute to the sputtered flux without a least one additional collision. Therefore, $\phi(E)/k\sqrt{E}$ will be neglected. This gives finally

$$p(E) = \frac{2}{kE^{5/2}} N\Phi \int_0^T E'\, d\bar{\sigma}(E_o,E') \quad . \tag{21}$$

The quantity $\int_0^T E' d\bar{\sigma}(E_o,E')$ is immediately recognizable from range theory

(Lindhard et al. 1963) as the nuclear stopping cross section denoted by $S_n(E_o)$. $S_n(E_o)$ when multiplied by the density of target atoms gives the nuclear stopping power. Recalling also that $k\sqrt{E} = N\sigma v$, we finally get for the density of moving atoms

$$p(E) = \frac{2\Phi}{\sigma v E^2} S_n(E_o) \tag{22}$$

Here $S_n(E_o)$ = nuclear stopping power of the target material for the incident beam

Φ = incident flux

σ = total cross section for target atom-target atom collisions (at energy E)

v = velocity of target atoms with energy E.

We now assume that the flux of particles with energy E inside the target is isotropic. If $F_i(E)$ is the flux of moving target atoms per unit solid angle inside the target, then

$$F_i(E) = \frac{p(E)v}{4\pi} = \frac{\Phi}{2\pi\sigma E^2} S_n(E_o) \quad . \tag{23}$$

Thus far, no mention has been made of surface binding effects. Thompson (1968) has shown that these effects dominate the energy distribution at small values of E. He assumed (Thompson 1968) a rectangular potential barrier at the surface and showed that the flux of target atoms per unit solid angle outside the target F(E) (that is, the sputtered flux) is related to $F_i(E)$ by

$$F(E) = \left(\frac{E}{E + E_b}\right) F_i(E + E_b) \cos\theta \tag{24}$$

where E_b = surface binding energy, and

θ = angle measured with respect to the surface normal.

If $S(E,\theta)$ is the sputtering yield per unit energy per unit solid angle expressed as a function of energy and angle to the target surface normal, then from equations (23) and (24)

$$S(E,\theta) = \frac{F(E)}{\Phi} = \frac{1}{2\pi\sigma} \frac{E}{(E+E_b)^3} S_n(E_o) \cos\theta \quad . \tag{25}$$

Integrating $S(E,\theta)$ over the hemisphere results in the expression

$$S(E) = \int 2\pi\, S(E,\theta)\, d(\cos\theta) = \frac{1}{2\sigma}\left[\frac{E}{(E+E_b)^3}\right] S_n(E_o) \quad . \tag{26}$$

The energy dependence of $S(E)$ that is obtained in this treatment is given by $E/(E+E_b)^3$. This is precisely the result that was obtained by Thompson (1968). The two dominant features that are evident are a linear decrease to zero at small energies and a quadratic decrease at high energies. The former is clearly an artifact of the surface binding given by equation (24). The latter is a result of the assumptions that went into the derivation of equation (13). Note that if S is the total sputtering yield, we can rewrite (25) as

$$S(E,\theta) = \frac{2}{\pi} S\left[\frac{EE_b}{(E+E_b)^3}\right] \cos\theta \quad . \tag{27}$$

The result obtained by Sigmund (1972b) is somewhat more general than the E^{-2} obtained by Thompson. Following Lindhard *et al.* (1963),

Sigmund (1972) assumed a cross section for target atom-target atom interactions of the form

$$d\bar{\sigma}(E_0,T) = CE_0^{-m} T^{1-m} dT \quad , \tag{28}$$

where C is a constant with dimensions of area multiplied by energy to the 2m power.

Using a transport equation approach, he showed (Sigmund 1972, 1972a, 1972b) that the energy spectrum of sputtered particles resulting from this assumption has the form E^{-2+2m} when surface binding effects are neglected. If one again assumes that the surface binding may be modeled as a rectangular potential barrier, as was done above, then this form leads to an energy spectrum

$$S(E,\theta) = \frac{2}{\pi} S(1-m)(1-2m) \left[\frac{EE_b^{1-2m}}{(E+E_b)^{3-2m}} \right] \cos\theta \tag{29}$$

Thus in deriving equation (27) Thompson, in effect, assumed m = 0. (It is interesting that one can identify the precise place in Thompson's derivation where the assumption was made. He assumed that the stopping power of a moving atom was proportional to E. However, the cross section given by equation (28) would predict that the stopping power was proportional to E^{1-2m} (Sigmund 1972). Since the energy spectrum he derived contained the stopping power as a factor in the denominator, he obtained E^{-2} rather than E^{-2+2m}.) The choice of a value of m in equation (28) is ultimately a choice of the form of the interatomic potential to be used. More will be said about this choice in the discussion of the results of the experiment.

In summary, one can make simple arguments to show that if atoms in a collision cascade share energy efficiently, the energy spectrum of moving atoms is proportional to E^{-2}. The effect of surface binding forces is to cause the spectrum of sputtered atoms to turn over and fall to zero at small energies.

III. EXPERIMENTAL APPARATUS

A. Design Considerations

A diagram of the time-of-flight spectrometer used in this experiment is shown in Figure 1. The duoplasmatron ion source produces an ion beam that is momentum selected by a 31° magnet before entering the spectrometer chamber. There it passes through an arrangement of two fixed slits 1.11 cm wide by 0.45 cm high. Between these slits is the rim of a rapidly rotating disk with two diametrically opposed slits of the same size as the fixed slits. During each rotation of the disk, each moving slit aligns itself momentarily with the fixed slits, allowing the ion beam to pass. The beam pulse so produced continues through a cold trap filled with liquid nitrogen into an ultra-high vacuum system (base pressure of $\simeq 5 \times 10^{-10}$ torr) where it strikes the target. Sputtered material ejected back in the direction of the beam passes through one of the fixed slits and is collected on the rotating disk.

In addition to the fact that this geometry allows the velocity spectrum to be measured normal to the target surface, it has two important practical advantages. First, since the beam pulse is caused by the moving collector, there is no possibility for the beam pulses and the rotating collector to get out of synchronization. Second, the time zero of the collected spectrum is uniquely determined by the geometry of the disk.

The design considerations of the apparatus for this experiment are similar to those described by Thompson *et al.* (1968). We consider a rotating collector of radius r, with rotation rate ν(rev/sec), at a

distance ℓ from the target being sputtered. In the time, ℓ/v, that it takes a sputtered particle with velocity v to reach the collector, the rim of the collector has rotated a linear distance of

$$x = \frac{2\pi r \ell \nu}{v} \equiv \frac{k}{v} \quad . \tag{30}$$

This equation defines the dispersion constant, k, whose value is a function of the apparatus design only. Like Thompson et al. (1968), we also assume that the beam pulse is some fraction, f, of the period of rotation of the collector. Furthermore, we take the width of the fixed slit which defines the trajectories of those sputtered particles which strike the collector to be $d = 2\pi rf$. Equating d and x gives an equation that may be viewed as defining the maximum velocity that can be resolved with a given apparatus, or, equivalently, as specifying the requirements that must be met by the apparatus to resolve a given velocity. The equation is

$$fv = \ell\nu \quad . \tag{31}$$

Before further consideration of this requirement, let us derive a condition for the dispersion constant itself. It is obvious that the amount of dispersion required to obtain a satisfactory velocity spectrum on the collector is related to the spatial resolution of the technique that is used to measure the amount of collected material as a function of position. In practice, any technique will measure the amount of material in some region of width Δx at a position x on the collector. Thus, a reasonable criterion that must be satisfied is that the dispersion constant, k, be sufficiently large that the fractional change in v

associated with the width Δx is below some specified tolerance when v is the maximum that is to be studied. Taking the derivative of equation (30) this condition is

$$\frac{|\Delta x|\ v_{max}}{|\frac{\Delta v}{v}|} \leq k \quad . \tag{32}$$

We have chosen to design the apparatus to resolve 1 keV ^{235}U which have a velocity of 2.85×10^6 cm/sec. The $|\Delta x|$ associated with the nuclear track technique used to detect the sputtered ^{235}U is about 0.02 cm. Picking 5% as a reasonable value of $|\Delta v/v|$ then requires that

$$k \gtrsim 1.14 \times 10^6 \text{cm}^2/\text{sec} \quad . \tag{33}$$

Returning now to the requirement (31),

$$\ell\nu \gtrsim 4.00 \times 10^4 \text{cm/sec} \quad , \tag{34}$$

where f has been chosen to be 1.4%. This choice is quite arbitrary at this point, although intuition suggests that a value around 1% is appropriate. (The precise effect that f has upon the final spectrum will be given in Section V.) Since the density of sputtered particles collected in a given time falls off as ℓ^{-2}, it is clear from equation (34) that ν should be chosen as large as is practical. A motor was found that attains a speed of 500 rev/sec. Therefore, ℓ was chosen to be $\simeq$ 80 cm, and as a result of (30) and (33), r had to be greater than 4.5 cm. In fact, r was chosen to be 5.08 cm, giving the apparatus a dispersion constant of $k = 1.30 \times 10^6 \text{cm}^2/\text{sec}$.

One final factor that must be considered in the apparatus design is the constancy of the motor speed. In order that the inherently high spatial resolution of the nuclear track technique not be wasted, it is necessary to place an upper limit, ΔT, on the allowable fluctuation in the revolution period, T, of the motor. Thus

$$\frac{\Delta T}{T} \lesssim \frac{\Delta x}{2\pi r} \quad . \tag{35}$$

For a rate of rotation $\nu = 1/T = 500$ rev/sec,

$$\Delta T \lesssim 1.25 \ \mu\text{sec}$$

or

$$\frac{\Delta T}{T} \lesssim 0.05\% \quad .$$

In addition, $\Delta\nu/\nu$ should also be $\lesssim 0.05\%$ instantaneously.

B. Hardware

Where the load conditions may vary, the simplest way to meet the requirement of a constant period of rotation is to select a hysteresis synchronous motor. Such a motor has the property that it remains in phase with the alternating current that drives it. Thus, the problem of maintaining a constant period of rotation for the motor is reduced to the problem of making a stable alternating current power source. The motor selected was a single phase two-pole hysteresis synchronous motor specified for 115 VAC operation at 500 Hz (manufactured by the F. C. Globe Co., Dayton, Ohio). During operation inside the vacuum system the motor's current requirement was about 0.2 A.

The requirement for long term frequency stability stated above suggested that the basic time standard for the system should be a quartz crystal controlled oscillator. The availability of an inexpensive integrated circuit crystal oscillator (MC 12060) requiring no external components except the crystal itself and providing a TTL (transistor-transistor logic) compatible output greatly simplified the construction of the stable 500 Hz signal source. For convenience a 1 MHz crystal was chosen. The resulting 1 MHz square wave signal from the oscillator was fed into a chain of type 7490 decade divider integrated circuits which had been wired to give a division of 2000 and a square wave output. The final stage of signal conditioning was a low-pass active filter with corner frequency chosen to pass the fundamental 500 Hz signal, but to attenuate the third and all higher harmonics. A buffer amplifier provided an adjustable output from 0 to 20V p-p.

In order to provide sufficient power at the proper voltage for operation of the motor, a power amplifier was constructed. This amplifier accepted the stable oscillator signal as input and was capable of delivering about one ampere at the specified 115 VAC. It was found that the motor required a large amount of power only during starting. In fact, after achieving rated speed, the voltage applied to the motor could be lowered to 90 VAC. This resulted in a lower operating current and consequently cooler operation.

As may be seen schematically in the insert at the lower right of Figure 1, the motor was mounted inside the vacuum chamber on a thick aluminum support. Water cooling of this motor mount kept its temperature at about 25°C during operation. This temperature was measured by a type

LX5600 solid state temperature transducer installed in a well in the aluminum near the motor. The output of this device (a constant 10 mV/°C) was monitored closely during motor operation, since a sudden temperature rise is likely to precede catastrophic failure of the bearings.

While a properly functioning hysteresis synchronous motor rotates in phase with the power driving it, preliminary experiments with a 12,000 RPM motor showed that a heavy or unbalanced load could prevent the rotor from achieving rated speed. For this reason, it was necessary to have the capability to independently measure the rate of rotation of the collection disk. The two slits located opposite each other on the rotating collector disk (see insert at upper left of Figure 1) provided a natural way to do this. An optical link (see Figure 2) consisting of an infrared-light-emitting diode and a silicon phototransistor was mounted inside the vacuum system in such a way that, as the motor turned, the moving slits allowed the optical link to be completed twice during each complete rotation of the collector. The resulting pulses were amplified and conditioned for TTL compatibility, and the period between successive pulses was monitored by a frequency counter operated in the period measurement mode. During a typical fifteen hour run, the mean and standard deviations of the hourly readings of this period were 999.97 μsec and 0.02 μsec, respectively. This clearly exceeds the stability requirements outlined above.

In the introductory paragraph of this section, the technique for creating the beam pulse was described. Clearly, during most of the rotation of the collection disk, the accelerator beam would be stopped by the disk itself. In order to prevent this, it was originally planned

to mount two disks on the motor shaft. The one nearest the uranium target was to be the collector of sputtered material, while the other was to be a beam-stop made of tantalum. It was found, however, that the motor was incapable of spinning this double disk arrangement at rated speed. As a result, an electrostatic beam chopper (see Figures 1 and 2) was included in the system.

The chopper consisted of two parallel plates about 50 cm in length and having a capacitance of about 15 pF. One of the plates was connected to ground and the other to +300V through a 1 kΩ resistor. This provided a +300V potential difference between the plates, and deflected the ion beam sufficiently that it did not reach the spectrometer. When a beam pulse was desired, a high voltage power transistor placed in parallel with the beam chopper plates was turned on. This shorted the plates and allowed the ion beam to pass undeflected. A driver circuit was built for the power transistor which provided for fast switching and a TTL compatible input signal.

The optical link described above originated a trigger signal for the beam chopper (see Figure 2). The logic output of the optical link was fed into a type 74121 monostable multivibrator which functioned as a time delay. This delay allowed the slit in the collector wheel to rotate from the position where it generated an optical signal to the position where it could generate a beam pulse. A second 74121 was placed in series with the first. This circuit was adjusted to deliver a pulse to the beam chopper driver which was slightly longer than the desired beam pulse. This arrangement resulted in the shorting of the chopper plates (and passage of the beam) during the short time that the fixed and moving

slits overlapped. The stability of the 74121 time delays was great enough that after initial synchronization no additional adjustments were required.

One additional problem with this technique for creating beam pulses should be mentioned. The bearings used in the motor electrically insulated the rotor and shaft from ground. As a result, the small amount of beam that struck the collector during each pulse could have built up high voltages on the rotor. Under these conditions sparks in the bearings would have been likely. Since such sparks would have had a disastrous effect on bearing integrity, it was necessary to provide a low resistance path from the motor shaft to ground. This was accomplished with a graphite brush supplied by the motor manufacturer.

As stated earlier in this section, the rotating collector was chosen to be 5.08 cm in radius. The original ones used in this experiment were fabricated from a standard alloy (2024) Al sheet 0.025 cm thick. However, these had two disadvantages. They were difficult to balance and they produced a background of fission tracks that was characteristic of an impurity of about 1 ppm uranium of natural abundance. Subsequent wheels were fabricated from 99.99% pure Al sheet 0.05 cm thick. The added thickness and softness of these disks facilitated dynamic balancing. In addition, they contributed a background of fission tracks that was about a factor of 4-5 lower than the previous models. The spectrum from the metal target was obtained with one of the original wheels, while that from the oxide target used a newer one.

The collector disks were mounted on a hub affixed to the motor shaft and dynamically balanced by a professional balancing company

(Khougaz Electrodynamic Balancing, 15960 Blythe St., Van Nuys, CA). As a final preparation before use, each disk was cleaned by a standard UHV procedure (Roth 1976), and lines were scribed on it to facilitate cutting (see Figure 3).

The ^{235}U metal and $^{235}UO_2$ targets used in this experiment were mounted in copper holders along with a quartz disk for viewing the beam. These target assemblies were mounted on a linear manipulator and placed in the UHV chamber indicated in Figure 1. This bakeable stainless-steel chamber has been described by Gregg (1977). The targets used in this experiment were not mounted in the main body of that chamber, but in a standard 2" stainless-steel cross attached to it. This location was chosen to minimize ^{235}U contamination of the vacuum system, and minimize the target to collector distance.

The final requirement to insure proper technical operation of this experiment was a method for monitoring the shape of the ion beam pulses arriving at the metal and oxide targets. In addition, it was necessary to integrate the beam current in order to determine when an appropriate amount of material had been sputtered. (Note, however, that because this experiment is sought only to determine the amount of ^{235}U sputtered at one energy relative to that at another, no absolute charge integration was required.) As a result of this requirement, an inverting unity gain current amplifier was placed in the beam current path between the target and the current integrator (see Figure 2). The current integrator thus saw the same current (with only a polarity change) that it would have seen if it had been connected directly to the target. Moreover, the operational amplifier (voltage) output (Figure 2) was compatible with an

oscilloscope input. It was found that this arrangement provided an integration error of less than 1%. The approximately triangular beam pulse shape expected on the basis of geometry was confirmed by the oscilloscope display.

It is a usual practice when integrating accelerator beam currents to bias the target at a positive voltage which may be as large as several hundred volts. The purpose of this bias voltage is to prevent the escape from the target of energetic electrons produced by the ion beam bombardment. It is obvious that the addition of such a bias voltage would alter the energy spectrum of any sputtered particles which were charged. For this reason no bias (battery) was used in this experiment. The integration error of less than 1% mentioned above referred to instrumental error and not to the absolute error in the determination of the ion beam current. It is believed that the measured current on the targets was somewhere between a factor of 2 and 10 larger than the true ion beam current because of these electrons. On the quartz, however, a +300V bias battery was observed to increase the measured current by about 10%.

A current integrator was constructed for this experiment and for general use with the 150 kV ion source. Its principles of operation and performance characteristics are discussed in Appendix B.

IV. EXPERIMENTAL PROCEDURE

A. Accumulation of Sputtered Material

The uranium metal target used in this experiment was a 93% enriched cold rolled ^{235}U foil 0.0025 cm thick and about 0.5 cm^2 in area, obtained from the Oak Ridge National Laboratory (Gregg 1977). Prior to being placed in the vacuum chamber it was dipped in 70% HNO_3 to remove most of the oxide layer (UO_2) formed by exposure to air. This etching process, lasting typically two to five minutes, was followed by a distilled water wash and a final dip in acetone. Following this operation the foil was mounted in the vacuum chamber as soon as possible in order to minimize additional oxidation.

The uranium oxide (UO_2) target was also prepared by the Oak Ridge National Laboratory. It was made from 93% enriched $^{235}UO_2$ powder by hot pressing. Cylindrical in shape, both its diameter and thickness were 1 cm. According to data supplied by ORNL, the UO_2 from which the pellet was prepared was composed of particles whose average size was 2.97 μm. It had 5.40 m^2 of surface area per gram and an oxygen to uranium ratio of 2.14. The water content was about 0.34%.

Immediately before beginning the collection of data, the metal foil target was sputter cleaned with the 80 keV $^{40}Ar^+$ beam. The d.c. current used during the cleaning run was about 3 μA (as measured on the quartz viewer), which for a sputtering yield of 2 (Gregg and Tombrello 1977) removed approximately 20 atomic layers of ^{235}U. During the sputter cleaning one of the slits in the collector was aligned with the fixed slits, thus allowing the beam to pass while preventing any ^{235}U from

hitting the collector surface. During the actual run, the rate of arrival of Ar^+ ions at the target was about $5.6 \times 10^{12} cm^{-2} sec^{-1}$. This flux is sufficient to remove a monolayer from the target about every 120 sec. The pressure of the target chamber during Ar^+ bombardment was about 4×10^{-8} torr; however, most of this was contributed by the Ar introduced by the beam. The chamber pressure without the beam present was about 4×10^{-9} torr. It is assumed that this represents the partial pressure of the gases that would be likely to contaminate the surface during the run. Even if these gases stuck to the target with 100% probability, the Ar bombardment would keep the target clean. Since the primary contaminant expected was oxygen, the $^{235}UO_2$ target was not presputtered. More will be said about the problem of contamination in Section V.

The first step in actually producing an energy spectrum was to obtain in the target chamber an analyzed and focused beam of the desired ion. For both spectra presented, the sputtering ion was $^{40}Ar^+$ at an energy of 80 keV. The ion source voltage was calibrated directly with a resistive divider and a precision digital voltmeter. Selection of the correct ion beam was accomplished by observing the voltage of a Hall effect generator placed in the fringe field of the 31° analyzing magnet (Figure 1). In order to extend the life of the ion source filament, the source gas used to obtain an Ar^+ ion beam was a mixture of 10% argon and 90% helium. The beam was focused by observing the fluorescence it produced when it was allowed to strike the quartz disk that was an integral part of the target assembly.

After obtaining a focused beam of adequate current (generally $\gtrsim$ 4 μA as measured on the quartz) and completing sputter cleaning, the

spectrometer motor was started. The motor starting current was about 560 mA at 115 VAC. Spinning up to rated speed usually required several seconds. After rated speed had been achieved, the voltage applied to the motor was lowered to 90 VAC to minimize heating, as stated previously.

The only device that required adjustment before sputtering of the target began was the analog delay pulser, which provided pulses to the beam chopper. The delay control was set for minimum delay and slowly increased until beam pulses began to appear at the target. The correct width of the pulses was obtained in a similar manner. After these adjustments were made, the beam was temporarily interrupted, the target put into place, and the irradiation begun. It was found that the average direct current arriving at the target was 1-2 μA. This is clearly in excess of that to be expected on the basis of the current as measured on the quartz, and confirms that a substantial number of secondary electrons were produced by both the uranium metal and the UO_2 targets.

The length of a sputtering run was determined by the number of collected sputtered atoms necessary to obtain an adequate signal above the uranium background present in the collector. The ratio of collected atoms to charge accumulated on the target was determined experimentally for the ^{235}U foil and the $^{235}UO_2$ pellet. This was necessary in view of the uncertainty in charge integration mentioned above. The units used in this determination were fission tracks per square centimeter per coulomb of integrated target current. The values calculated assumed that the fluence of thermal neutrons used in the ^{235}U detection process was

$10^{16}cm^{-2}$. The particular density of fission tracks referred to is the maximum to be expected in the energy spectrum. Thus, for the metal foil a maximum track density of 1.63×10^{7} tracks/cm^2/C was expected, while for the pellet the corresponding number was 1.79×10^{7}tracks/cm^2/C. (The relative sizes of these numbers is surprising but probably not significant. Obtaining well focused beam spots with the 150 kV ion source is very difficult. It is likely that some beam hit the holder of the ^{235}U metal target, since it was rectangular. By contrast the UO_2 target was circular.) For ease of counting, a maximum density of tracks of about $10^{6}cm^{-2}$ was desirable. The fluence of $^{40}Ar^{+}$ ions which produced this maximum proved also to give adequate numbers of tracks in the low density regions of the spectra. As an example, consider the $^{235}UO_2$ pellet. Since a maximum density of tracks of $10^{6}cm^{-2}$ was desired, the required charge was 0.056 coulombs per spectrum. Because two spectra were accumulated simultaneously, sputtering continued until a total of .112 coulombs of charge was accumulated. The time required to complete this run was about 25 hours.

As was mentioned earlier in this section, it was important that the pressure in the target region be low enough that the surface of the target remained clean. It was also important that the pressure along the path of sputtered particles from the target to collector be low enough that collisions were improbable. The effect of such collisions will be considered further in the discussion of possible errors. The pressure in the motor chamber during runs was always less than 6.0×10^{-5}torr, with readings of $2\text{-}3 \times 10^{-5}$torr being typical. The pressure was highest immediately after the motor warmed up. In fact, once it was necessary to run

the motor for about an hour on the two days preceding the taking of data in order to outgas it. It should be noted, however, that the presence of the fixed slit (Figure 1) provided a considerable pumping impedance between the motor chamber and the in-line cold trap. As a result, virtually all of the flight path of the ^{235}U particles was in a region assumed to be at a much lower pressure. (Since the completion of the work described in this thesis, additional pumping has been added in the vicinity of the spectrometer chamber. This is expected to result in an improvement of about a factor of ten in the pressure there.)

B. Analysis of Sputtered Material

After the sputtering was completed, the collector disks were removed from the vacuum system and cut with a sheet metal shear along the lines shown in Figure 3. Cutting the wheel was a practical necessity dictated by the size of the center vertical access port of the UCLA research reactor. The maximum diameter of the package that could be irradiated there was somewhat less than five centimeters.

After cutting, the segments of the rim of the collector containing the ^{235}U (Figure 3) were placed in contact with mica sheets (1-1/2" x 2" x .001") which were used as fission fragment track detectors (Gregg et al. 1977). After each aluminum segment was placed in contact with a mica detector, a scriber was used to trace the segment's outline. In this way, the precise location and orientation of the segment could later be reconstructed. All six pairs of collectors and detectors were stacked in a specially constructed lucite plastic box which held them during the irradiation. In early runs a piece of NBS-612 glass containing

37.38 ppm uranium depleted to 0.2392 atom% was also included in the reactor package as a standard for calibrating the neutron fluence. It was found, however, that the accuracy of flux measurements made at UCLA was adequate to insure a suitable neutron exposure. As a result, in later runs no standard glass was used. All reactor runs were timed to give a neutron fluence of $10^{16} cm^{-2}$. This required two hours fifty-two minutes exposure in the maximum flux region of the reactor running at full rated power of 100 kW. Since the thermal neutron fission cross section of ^{235}U is 580 barns, about one ^{235}U in every 1.72×10^5 underwent fission.

The mica used as a fission fragment track detector was Indian ruby mica. The only preparation necessary before using it was the exposure of a fresh surface. This was usually accomplished by covering the mica with 2" wide cellophane tape. When the tape was removed, a few layers of mica were removed with it, leaving the desired fresh surface. The advantages of mica, and in particular Indian ruby mica, as a track detector for ^{235}U have been discussed by Gregg (1977). The most important one to this experiment is that the background of tracks caused by uranium within the mica is negligible.

The mica detectors could not be handled for about five days after their irradiation because of radioactivities produced by neutron activation of their constituents. At the end of this period the reactor package was disassembled and the micas etched in 48% HF. Initially, an etching time of ten minutes was chosen. It was found, however, that track counting was easier if the etching time was lengthened to twenty minutes. The effect of this extra time was to make the tracks thicker

and more readily distinguishable from natural blemishes and pits in the mica. Following the HF etch, the micas were placed in concentrated NH_4OH for about five minutes. The purpose of this bath was to neutralize the acid. Following the NH_4OH bath, the micas were given a running water wash for at least an hour. The last step in preparing the micas was removing them from the water wash and mounting them on microscope slides. Before they were actually affixed, however, they were washed with an organic solvent (usually acetone, although ethanol was used occasionally) as a final cleaning.

The track counting in this experiment was done using an optical microscope at a magnification of 450X. The microscope that was used had a precision movable stage that allowed the mica to be positioned in both horizontal directions (x and y) to the nearest 0.01 mm. The area in which tracks were counted for any given setting of the stage controls was determined by a square grid that covered most of the total viewing area. The center of this grid of one hundred small squares was conventionally taken to be the point whose coordinates were given by the stage micrometer readings. The area of the field of view was $3.6 \times 10^{-4} cm^2$. A reference point, or origin, was scratched in the mica at a convenient place away from the track covered area. The coordinates of this point were recorded and used as a reference for repositioning the mica in the event it had to be removed from the stage before counting was complete.

The first step in the counting process was to establish the location of the track covered area. As was pointed out earlier, when each section of aluminum collector was placed in contact with the mica detector, a scriber was used to scratch the outline of the collector. With

the microscope magnification at 100X, coordinates of various points on these lines were recorded. When these coordinates were plotted on a graph and lines were drawn through them, the outline of the original aluminum sample was reconstructed.

Since the collector was rotating, it is clear that the ^{235}U atoms with any given velocity will lie along a radius of the collector disk. Further, the velocity will be related to the angle of this radius with respect to a chosen reference radius. The radius always chosen as reference was the one that bisected the slit through which the beam passed (Figure 3). This radius corresponded to zero flight time from the target to the collector. In order to sample a given velocity, microscope fields had to be chosen that were along a radius of the original collector that formed a known angle with the reference radius.

The first step in calculating the coordinates of the microscope fields to be counted on any detector was to determine the coordinates of the point corresponding to the center of the aluminum collector. Since three non-collinear points uniquely determine a circle, it was natural simply to select the coordinates of three widely spaced points on the curved scribed line (see Figure 3) and from them infer the center. However, because any segment subtends at most 60° of arc and because of the possibility of deviations when the curved segment was being scribed on the mica, this technique proved to be unreliable. A possible improvement that was considered was to select several combinations of three points on the curved line and from each combination imply a center. The various values obtained were then averaged. This

procedure, however, was also flawed because many of the combinations chosen subtended far less than the 60° mentioned above and, therefore, were even less reliable. The solution chosen was to use all the points that were recorded along the curved line simultaneously and find the best circle in a least squares sense. This procedure yielded the coordinates of the center of the circle that best matched the curved scratch in the mica. The circle's radius was also obtained. This radius could be compared with the known radius of the collector disk as a check of consistency. The equations that must be solved in order to fit points to a circle in the least squares sense are

$$x - \frac{1}{n}\sum_i x_i + \frac{r}{n}\sum_i \frac{x_i}{r_i} - \frac{xr}{n}\sum_i \frac{1}{r_i} = 0 \quad ,$$

$$y - \frac{1}{n}\sum_i y_i + \frac{r}{n}\sum_i \frac{y_i}{r_i} - \frac{yr}{n}\sum_i \frac{1}{r_i} = 0 \quad ,$$

and

$$r = \frac{1}{n}\sum_i r_i \quad . \tag{36}$$

Here $r_i^2 = (x_i - x)^2 + (y_i - y)^2$

(x,y) = coordinates of the circle center (unknown)

r = radius of the circle (also unknown)

and

(x_i, y_i) = coordinates of i^{th} data point.

The number of equations was reduced from three to two trivially by substituting the value of r from the third equation into the first two. An iterative technique was then used to solve the remaining pair of

equations. On the basis of a center calculated from three widely spaced points, a guess for the correct y value was made. Using this value, the first equation above was solved to give a value of x. In turn, this x value was used in the second equation to predict a better value of y. The iteration continued until values of x and y were obtained that were of sufficient accuracy for calculations. This accuracy was taken arbitrarily to be 0.001 mm. Usually about four to six iterations were required. A programmable calculator was used to do the calculations. The values of r calculated by this procedure were usually within $\sim$0.5 mm of the expected value.

The second step in calculating the coordinates of the microscope fields to be counted was to establish the orientation of the track covered area by finding the angle formed by the long straight side of the segment (that is, the scratch on the detector corresponding to it) and the microscope x axis (see Figure 3). To do this, the data points that were taken on each of the straight scratches of the segment outline were fit in the least squares sense by straight lines, and the angles with respect to the x axis of these lines were calculated. For each segment there were at least two independent determinations of the desired angles, since for each segment at least one of the short sides made an angle of 120° with the long one. The value chosen was the average of these. The differences that occurred were the result of small errors in the cutting process. They were typically less than 1° with one extreme example being 1.4°. The particular segment for which an angular error has the greatest effect is the one that contains the high energy portion of the spectrum. For these, the

maximum differences in the angle as calculated from the two independent sides was less than 0.5°.

Using the center coordinates calculated as above and the initial angle derived from the angles of the straight scratches with respect to the coordinate axes, the coordinates of four points along each of several equally spaced radii were calculated. These points were separated radially by 2.22 mm with the nearest to the center being 41.91 mm away from it.

Initially, track counting was done in transmitted light. Later, however, reflected light was used. (The choice is largely a matter of taste on the part of the individual who is counting.) Occasionally, a field was counted twice in order to test the reproducibility of the counting process itself. In early runs, where the HF etching time was ten minutes, the error was perhaps as large as 4%. Increasing the etching time to twenty minutes made the tracks more distinctive in appearance and reduced errors in track recognition to perhaps 2%.

Uranium impurities in the aluminum collector and the mica itself contributed a background of fission tracks that had to be subtracted. The level of this background was established by counting fields located on the detector in the area that was in contact with the portion of the Al segment outside the band exposed to sputtered ^{235}U (see Figure 3).

V. DATA AND DISCUSSION

A. Mathematical Analysis of the Spectrometer

Before presenting the results of the energy spectrum measurement, it is necessary to consider in greater detail the operation of the spectrometer in order to be able to recognize any aberrations that the measurement process might have introduced. An ideal time-of-flight spectrometer differs from any practical device in two ways. In the ideal spectrometer, beam pulses are very short, that is, Dirac delta functions of time. Further, the width of the slit that defines the particles that are collected is vanishingly small. This means that the correspondence between any location on the collector and the velocity of the particles that can strike there is unambiguous. In fact, neither of these conditions can be met in a real apparatus. The purpose of the following discussion is to assess quantitatively the effect of finite pulse and slit widths on the spectrum obtained.

Because it is common in the literature of sputtering to consider energy distributions rather than velocity or arrival time distributions, we shall take as the starting point of this discussion the sputtering yield per unit energy per unit solid angle, $S(E,\theta)$, where the angle θ is measured from the normal to the surface being sputtered. For the geometry of the spectrometer being considered here, θ is equal to zero because the target plane is chosen to be perpendicular to the beam. Define, therefore, $S(E,0) \equiv S(E)$. Now since the collector is located a distance ℓ from the target, the number of particles arriving per unit area in the energy range dE about E is $\phi(E)$ and

$$\phi(E) = \ell^{-2} S(E) \quad .$$

If the beam particle that gives rise to these sputtered particles strikes the target at t = 0, then the energy of a particle of mass m is related to its arrival time at the collector by

$$E = \frac{1}{2} m(\frac{\ell}{t})^2 \quad . \tag{37}$$

This relation may be used to change variables in the expression for $\phi(E)$. Thus

$$\phi'(t) = \ell^{-2} S[E(t)] \left| \frac{dE(t)}{dt} \right| \quad . \tag{38}$$

This quantity, $\phi'(t)$, is the flux of sputtered particles that arrives at the collector at time t, per beam particle incident at time t' = 0. For a beam pulse of finite duration the total flux at time t is given by the convolution

$$g(t) = \int_{-\infty}^{t} f'(t') \phi'(t-t') \, dt' \quad . \tag{39}$$

where f'(t') is the intensity of the beam at time t'. The density of particles at any location y on the wheel, p(y), is the integral of this flux over the finite time period that the point is exposed by the slit, that is, from

$$t_1 = \frac{y - \frac{1}{2} d}{u} \quad \text{to} \quad t_2 = \frac{y + \frac{1}{2} d}{u} \quad , \tag{40}$$

where u is the linear velocity of the collector at the rim. Hence,

$$p(y) = \int_{\frac{y-\frac{1}{2}d}{u}}^{\frac{y+\frac{1}{2}d}{u}} dt \int_{-\infty}^{t} f'(t')\,\phi'(t-t')\,dt' \quad . \tag{41}$$

It is convenient to measure y in units of the slit width, $d = 2\pi rf$. That is,

$$y = zd$$

and

$$p(z) = \int_{(z-\frac{1}{2})\frac{d}{u}}^{(z+\frac{1}{2})\frac{d}{u}} dt \int_{-\infty}^{t} f'(t')\,\phi'(t-t')\,dt' \quad . \tag{42}$$

It is also convenient to measure time in units of 1/2 the pulse width $t_0 = fT$. So let $t = xt_0$, and let the primed functions f' and ϕ' become unprimed ones upon change of variables. This change yields

$$p(z) = \int_{(z-\frac{1}{2})\frac{d}{ut_0}}^{(z+\frac{1}{2})\frac{d}{ut_0}} dx \int_{-\infty}^{x} f(x')\,\phi(x-x')\,dx' \quad . \tag{43}$$

Finally, note that

$$\frac{d}{ut_0} = \frac{2\pi r}{uT} = 1 \quad . \tag{44}$$

Thus, the final expression for the density of collected sputtered material becomes

$$p(z) = \int_{z-\frac{1}{2}}^{z+\frac{1}{2}} dx \int_{-\infty}^{x} f(x')\,\phi(x-x')\,dx' \quad . \tag{45}$$

In this experiment the pulse shape was approximately triangular and centered at t = 0. Thus,

$$f(x) = \begin{cases} 1 - |x| & , \quad |x| \leq 1 \\ 0 & , \quad |x| > 1 \end{cases} , \tag{46}$$

is the normalized pulse shape. Let us now consider a specific example of this formula.

Recall from equation (27), that the random collision cascade model gives an expression of the following form for $S(E,\theta)$,

$$S(E,\theta) = \frac{2}{\pi} S \frac{EE_b}{(E+E_b)^3} \cos\theta \tag{47}$$

where S is the total sputtering yield and E_b is a surface binding energy which is usually taken to be the sublimation energy. For our experimental configuration and the spectrum given by equation (47):

$$\phi(x) = \left(\frac{S}{\pi \ell^2}\right) \frac{4x_0^4 x}{(x^2 + x_0^2)^3} \equiv \frac{S}{\pi \ell^2} \lambda(x, x_0) \tag{48}$$

where

$$x_0^2 = \frac{\frac{1}{2} m \left(\frac{\ell}{t_0}\right)^2}{E_b} \equiv \frac{E_0}{E_b} \tag{49}$$

m = mass of sputtered particle,

t_0 = fT = 28 μsec,

T = rotation period = 2 ms,

ℓ = target-collector distance = 81.3 cm for the ^{235}U metal target
81.7 cm for the $^{235}UO_2$ target

and E_b = surface binding energy of ^{235}U.

This defines the function λ. x_o may be thought of as the time (in units of t_0) that it takes a particle of energy E_b to travel from the target to the collector. For our apparatus E_0 = 1040 eV for the U target spectrum and 1051 eV for the UO_2 target spectrum. (Slightly different target-collector distances are responsible for the difference.) For numerical calculation it is convenient to note that particles that strike the collector at position z have energy

$$E = \frac{x_0^2}{z^2} E_b = \frac{E_0}{z^2} \quad . \tag{50}$$

Although tedious, it is possible to carry out the integral (45) analytically for the functions (46) and (48). The result is

$$p(z) = \frac{S}{\pi \ell^2} [\gamma(z,x_0) + \varepsilon(z,x_0)] \tag{51}$$

where

$$\gamma(z,x_0) = \frac{x_0^2}{2} \sum_{n=0}^{3} (-1)^n \binom{3}{n} \left(\frac{z + n - \frac{3}{2}}{x_0}\right) \tan^{-1}\left(\frac{z + n - \frac{3}{2}}{x_0}\right) \; ; \; z \geq \frac{1}{2} \tag{52}$$

and

$$\varepsilon(z,x_0) = \begin{cases} \frac{x_0^2}{2}\left[\left(\frac{z - \frac{3}{2}}{x_0}\right)^2 - \left(\frac{z - \frac{3}{2}}{x_0}\right) \tan^{-1}\left(\frac{z - \frac{3}{2}}{x_0}\right)\right] & ; \; \frac{1}{2} \leq z \leq \frac{3}{2} \\ 0 & ; \; z > \frac{3}{2} \end{cases} \tag{53}$$

Here $\binom{3}{n}$ is the binomial coefficient $\binom{3}{n} = \frac{3!}{n!(3-n)!}$

Only the region $z \geq 1/2$ is of interest, since the slit in the rotating collector is located in the region $-1/2 \leq z \leq 1/2$. The function $\gamma(z,x_0) + \varepsilon(z,x_0)$ is the spectrum that would be obtained by the spectrometer used in this experiment if an ideal spectrometer obtained $\lambda(z,x_0)$. The two expressions $\gamma(z,13.9) + \varepsilon(z,13.9)$ and $\lambda(z,13.9)$ are plotted in Figure 4. Over the entire range of z, the two curves are practically indistinguishable. The value $x_0 = 13.9$ is chosen on the basis of a sublimation energy of $E_b = 5.4$ eV (Gschneidner 1964). The conclusion that can be drawn from Figure 4 is that the spectrometer does not introduce systematic error into the measurement in spite of its non-ideal nature.

If p(z) is an arrival time spectrum measured on an ideal spectrometer, then the corresponding energy distribution is given by the inverse of equation (38):

$$S(E) = \ell^2 p[z(E)] \left|\frac{dz(E)}{dE}\right| \quad , \tag{54}$$

Since

$$E = \frac{1}{2} m\left(\frac{\ell}{t_0}\right)^2 \frac{1}{z^2} = E_0 z^{-2} \quad . \tag{55}$$

Parametric equations for S(E) and E are

$$S(E) = \frac{\ell^2}{2} \frac{z^3}{E_0} p(z) \quad \text{and} \quad E = \frac{E_0}{z^2} \quad . \tag{56}$$

We have seen how the deviation of the spectrometer from ideal behavior alters the arrival time distribution. In order to judge the

systematic error in inferring S(E) from non-ideal spectrometer data, the distribution $p(z) = \ell^{-2}[\gamma(z,13.9) + \varepsilon(z,13.9)]$ has been inverted according to equation (56). Let S'(E) be the result of this process. The true S(E) that leads to this p(z) is known to be equation (47) with $(S/\pi)\cos\theta = 1$. S'(E) is plotted as the dashed curve in Figure 6. Over the entire range shown S'(E) differs from S(E) by less than the width of the line. Clearly, it is reasonable to take

$$S(E) = S'(E) \quad . \tag{57}$$

Thus far, it has been assumed that no time is required for the ion beam to travel from the collector wheel to the target. This, of course, is not right. In fact, it takes about 1.3 μsec for an 80 keV $^{40}Ar^{+}$ beam to travel 80 cm, and this amounts to a shift in the origin of z of about 0.046. A shift of this magnitude is roughly comparable to the errors in determining z and, for this reason, it has been neglected. In other circumstances, however, this might not be justified. An example of such a case would be sputtering by a heavy, low energy projectile.

B. Presentation of Data

Figure 5 shows the measured distribution, N(z), of sputtered ^{235}U fission tracks for the ^{235}U metal target. Recall that z is dimensionless and may be understood either as the position on the rim of the collector in units of the slit width (d = 0.447 cm) or as the arrival time in units of 28 μsec. The distinct peak at an arrival time of about 112 μsec corresponds to a velocity of 7.26×10^{5} cm/sec. The error bars

shown are statistical. Each point in the peak represents over two thousand counted tracks. Apart from the single peak the spectrum is apparently devoid of structure. The result of inverting the data according to equation (56) is shown in Figure 6 as a collection of data points with statistical error bars. A power curve fit to the data points above $\sim$ 200 eV indicates that the behavior is about $E^{-1.77}$. For this reason the data were fit with a curve of the form

$$S(E) = A \frac{E}{(E+B)^{2.77}} , \tag{58}$$

where A is simply a constant scale factor. The smooth curve in Figure 6 is a graph of this function. A value of B = 5.4 eV (the sublimation energy) was found to give a good fit. A was taken to be 3.83 for normalization.

Figures 7 and 8 are the arrival time and energy distributions, respectively, for ^{235}U sputtered from the $^{235}UO_2$ target. Note the similarity to Figures 5 and 6. The most noticeable difference is that the distribution of ^{235}U sputtered from the oxide target seems to be shifted slightly toward lower energies. This is apparent in Figure 7 as a shift of the peak toward longer arrival times (larger z) and in Figure 8 as both a lower energy peak and a faster decrease with energy ($E^{-1.86}$ at large E). Unfortunately, a single curve such as equation (58) does not represent the $^{235}UO_2$ target data very well.

In order to facilitate comparison of Figures 6 and 8, the data from each have been reproduced without error bars in Figure 9.

C. Examination of Errors

Because of the small probability that any given ^{235}U nucleus will fission during neutron exposure, the Poisson distribution correctly describes the distribution of the number of tracks counted in any field of view about the theoretical mean. As a result, if N tracks are counted for a given data point, the error assigned is $\sqrt{N}$ (Gregg 1977). These errors are indicated by error bars in Figures 5, 6, 7 and 8. In addition to the statistical errors, there are three obvious sources of possible systematic errors. These are the attenuation of particles in flight by collisions with the residual gas, the sticking probability of ^{235}U atoms that strike the Al collector, and the determination of the dimensionless parameter z.

Consider first the sticking probability. Thompson et al. (1968) found that for gold atoms incident on steel the sticking probability was about unity, independent of energy. Measurements of the effective sticking probability of sputtered ^{235}U on aluminum (integrated over all energies) have been made recently in the Kellogg Laboratory (Griffith et al. 1978). They indicate that more than 97% of all ^{235}U sticks. In these measurements an $^{40}Ar^{+}$ beam was used to sputter ^{235}U from a metal foil target. The collector was essentially a closed volume with a small hole to admit some of the ^{235}U. Most of the atoms stuck to the first surface that they hit. Some ^{235}U, however, was found to be located at other places within the collection cage. In fact, it was found that this "non-sticking fraction" tended to be concentrated near the normal to the first collection surface. In the absence of experimental data or a

compelling theoretical prediction of the sticking fraction as a function of energy, the data of our energy spectrum experiment must be accepted with some qualification. The data of Arifov et al. support this view. They have measured the sticking probability of K^+ and Cs^+ ions with energies 3 to 40 eV on a single crystal Mo target. They found that for perpendicular incidence all ions with energies below $\sim$3 eV were retained by the surface. For larger energies, however, an increasing fraction was not retained. In fact for 40 eV about 70% of K^+ and 30% of Cs^+ ions did not stick. To put this in perspective, consider Figure 15. There the fraction of particles with energy less than E is plotted as a function of E for the distribution given by equation (58). It is clear from this curve that if the non-sticking particles were predominantly high in energy a significant distortion of the spectrum could be produced by relatively few of the total number of sputtered atoms. For this reason, a measurement of the sticking probability as a function of energy for uranium striking aluminum should be pursued with high priority.

In order to estimate the attenuation of the sputtered particles by the residual gas in the vacuum system, a test was conducted in which collectors were placed 80.2 cm and 25.8 cm away from the ^{235}U target. On the basis of geometry alone, the ratio of track densities obtained on these collectors should be 0.103. In order to simulate the conditions during a velocity spectrum measurement, the sputtering was done at a pressure in the target area of about 2×10^{-8} torr. The track densities obtained on the near and far collectors were 1.87×10^6 tracks/cm^2 ($\pm$ 3%) and 1.90×10^5 tracks/cm^2 ($\pm$ 3%), respectively, giving a ratio of 0.102,

which was essentially equal to the value predicted on the basis of geometry alone. (Even at a pressure of 3×10^{-6} in the target area, a deficit in the ratio of track densities of only 19% was observed.) These data suggest that aberrations introduced by this effect are minimal. As a further check on the consistency of this result, an estimate of the sputtering yield, S, of ^{235}U metal was made on the basis of the track density on the near collector. A value of 2 ± 1 was obtained, in agreement with the value obtained by Gregg and Tombrello (1977). (The large error in this number arises from uncertainties in the absolute magnitude of the neutron fluence and argon beam charge integration. Note, however, that neither of these possible errors affects either the energy spectrum or attenuation measurement, since both are relative measurements.)

A third source of possible error is in the determination of the value of z. A careful analysis of the boundaries of the track covered regions on the mica collectors indicates that this error is $\lesssim 0.1$ for the ^{235}U spectrum and $\lesssim 0.03$ for the $^{235}UO_2$ spectrum. (Note that z is dimensionless.) Errors of these magnitudes are not perceptible in the arrival time spectra of Figures 5 and 7, but may be important in the energy spectra of Figures 6 and 8, since both E and S(E) depend strongly on z. Equation (56) may be used to show that the effect of an uncertainty δz in z is to move the data points in Figures 6 and 8 along lines with constant slope -3/2 by distances that are proportional to $\delta z/z$. Points in the high energy region are clearly affected most, since z is smallest there; however, in Figure 6 the tendency is to move points approximately along the solid line, since its slope is $\sim$-1.77. Thus,

errors in determining z do not strongly affect the slope, n, of the curves in Figures 6 and 8. n is defined by the relation

$$n \equiv \frac{d[\ell n\ S(E)]}{d(\ell n\ E)} = -\frac{3}{2} - \frac{z}{2}\ \frac{dp/dz}{p} \quad , \tag{59}$$

where the expression on the right is obtained by using equation (56). An error δz in z will produce an error δn in n of

$$\delta n = -\frac{1}{2}\left(\frac{dp/dz}{p}\right)\ \delta z \quad . \tag{60}$$

Since the error, δz, is ≤ 0.1 and $(dp/dz)/p$ from Figure 5 is about 0.54, $\delta n \lesssim 0.03$ for the metal target spectrum. For the UO_2 target spectrum the smallness of δz makes δn insignificant. This confirms the qualitative conclusion stated above.

Perhaps the most important single consideration in any sputtering experiment is the condition of the surface being sputtered. This is particularly true when considering the lower range of ejection energies where most particles are emitted. The two targets used in this experiment, ^{235}U metal and $^{235}UO_2$, present problems that are, in a sense, complementary. Uranium is a reactive element which, when heated sufficiently, can burn in air. When exposed to air at ordinary temperatures it oxidizes progressively. An oxide layer forms on a fresh surface so rapidly that it is impossible to remove an existing oxide layer and mount a sample in vacuum without an unacceptably thick new oxide layer forming. This is the rationale for the preliminary sputter cleaning run that has been described. It is important to note, however, that even

in the vacuum system at a pressure of 10^{-9} torr, the oxidation continues. When an experiment is in progress for from 15 to 25 hours, as this one was, the best that can be hoped is that an equilibrium will be established in which the surface condition as a whole is relatively static and the amount of surface contamination that accumulates between beam pulses is small. In a sputtering yield measurement, one can test for the effects of surface contamination by varying the current of the sputtering beam over a wide range. Any tendency for the sputtering yield to change at lower currents is almost certainly due to contamination. (This problem is particularly acute in situations where the sputtering rate is low.) It would clearly be of use to apply to this experiment the procedure of varying the intensity of the sputtering beam. It has not been possible to do so, however, for obvious practical reasons.

The problem in sputtering the oxide target is more complex. It too is subject to contamination, but, in addition, it is possible that the surface may be altered chemically by ion bombardment. For this reason no presputtering of the $^{235}UO_2$ target was performed. Finally, the effect of the ^{40}Ar itself should be mentioned. After it has come to rest within the target, it constitutes a contaminant which could affect the outcome of the experiment. To test the validity of this idea, additional spectra should be measured with different bombarding beams. Ideally, a uranium beam should be used, since it would be indistinguishable both chemically and in mass from the target. Unfortunately, such a beam is not available at the present time. To summarize, the target

surface condition strongly affects the outcome of a sputtering experiment. Because of the duration of this experiment, surface characterization was particularly difficult.

D. Discussion of Results

Chapman et al. (1972) have identified four mechanisms that contribute to sputtering. They are surface recoils, thermal spikes, focused collision sequences, and random collision cascades. The first of these mechanisms is a two-collision event in which the incident beam ejects a surface atom which is then deflected by a neighboring surface atom into the direction of the collector. In this experiment such a mechanism cannot directly contribute, since the collector is located at 180° with respect to the incident argon beam direction. The second mechanism, thermal spikes, is thought to contribute to the sputtering of a metal like uranium, primarily when the target is at elevated temperatures (Chapman et al. 1972). Since the ^{235}U target in this experiment was at room temperature, this mechanism, which would contribute primarily at energies less than 1 eV, is not thought to be important in the interpretation of Figure 6. Of the remaining mechanisms, the random collision cascade is expected to be dominant. Its predicted spectral shape (equation (27)) is seen in Figure 6 to agree rather well with the data. There is, however, a systematic tendency for the data to decrease more slowly at higher energies than the model prediction. One possible explanation for the observed deviation could be the existence of focused collision sequences within individual crystals of the polycrystalline target. Thompson (1968) has concluded that the energy spectrum of

particles from focused collision sequences is proportional to E^{-1} for energies between the surface binding energy and the maximum energy at which a focused sequence can take place. The addition of a component with such a functional dependence on E might cause the observed behavior at higher energies. It should be pointed out, however, that our targets were subjected to a considerable amount of radiation damage. Whether or not enough crystal structure remained near the surfaces of individual grains to support focused collisions is uncertain. In addition, there is no evidence for a bend in the data that would be characteristic of the maximum focusing energy. This suggests that randomly oriented focused collision sequences are not a major factor in producing the observed deviation.

Another possible explanation for the deviation in the asymptotic slope of the data in Figure 6 from the prediction of equation (27) has been suggested by Sigmund (1972b). As discussed in the theory section, he assumed cross sections for interaction between target atoms of the form given by equation (28), and showed that the energy spectrum of sputtered particles that resulted had the form E^{-2+2m} when surface binding effects were neglected. When these surface effects were modeled as a rectangular potential barrier, as Thompson did in deriving equation (27), then the result was equation (29). Note now that equation (29) has precisely the form of the empirical fit (equation (58)) if $m \simeq 0.11$.

In choosing a value for m in equation (28) to represent collisions in a collision cascade, one is implicitly making a statement about interatomic potentials. Robinson (1970) has inverted equation (28) to obtain those potentials. He found that equation (28) successfully

describes Born-Mayer scattering with m = 0.05 and that smaller values of m give harder collisions. It is suggested that at least part of the deviation of the data in Figure 6 from the prediction of equation (27) may be traced to an assumption about interatomic potentials, and may reflect a need to refine that assumption.

A final possible mechanism to account for the deviation of the asymptotic slope from the random collision cascade prediction has been suggested by Thompson (1968) and explored quantitatively by Williams (1976). In both the model proposed by Thompson and the theory of Sigmund, the target was assumed to be an infinite medium. The observed sputtered flux from a real surface was assumed to be equal to the flux through an imaginary surface in this infinite medium. As Thompson (1968) pointed out, this assumption will tend to overestimate the flux of low energy particles. Williams considered this point in greater detail and found from his treatment that the energy spectrum from a target with a plane surface had the approximate form $E^{-1.7}$ (Williams 1976). In obtaining this result he used the hard sphere approximation for the scattering of target atoms.

Thus far nothing has been said about the spectrum of Figure 8. The theoretical models discussed so far all assume that the target is composed of only one kind of atoms. Kostin (1965) and Andersen and Sigmund (1974), on the other hand, have considered the problem of a two-component system. Kostin assumed hard sphere collisions and found that for a system where the mass of one component is much less than the mass of the other, the collision density of the heavy component has the form $aE^{-2} + bE^{-2+k}$. Here a and b are determined by the initial conditions

and k depends upon the mass ratio of the components, their number densities, and various cross sections for collisions. For a system composed of UO_2, k is about 0.6.

Andersen and Sigmund (1974) use an equation equivalent to the one used by Kostin, but use cross sections similar in form to equation (28). They find that the resulting spectra have the form E^{-2+2m_i}, where m_i plays a role equivalent to m in equation (28). Values of m_i in the range of 0.055 to 0.33 are considered with smaller values usually being associated with the heavy constituent. An examination of Figure 9 shows that the spectrum from the oxide target (filled circles) seems to fall below the spectrum from the metal target (open triangles) at higher energies. The effect, however, is small.

Another noticeable feature of the oxide target spectrum is that it is peaked at a lower energy than its metal target counterpart. From the arguments discussed previously, one would expect this lower energy peak would imply a lower surface binding energy E_b, since in the usual (E^{-2}) theory the peak occurs at 1/2 E_b. However, using measured total sputtering yields, and Sigmund's theory, Kelly and Lam (1973) have found an effective E_b of $\sim$ 8-11 eV. This apparent discrepancy may be due to a deficiency in the experimental data or to a failure of the theory when used for compound targets. A careful measurement of the sputtering yield of ^{235}U from the target used for the energy spectrum measurement would be of interest in this regard.

Miyagawa (1973) and Können et al. (1974) have reported experiments designed to measure the energy spectrum of material sputtered from alkali halide targets. Miyagawa (1973) found, using a time-of-flight scheme,

that the spectrum of the sputtered Na^+ ions from an NaCl target has a peak at about 2 eV and decreases as E^{-2} at energies above about 10 eV. Können et al. (1974) investigated the spectrum of both the alkali and halogen atoms and found that the spectra did not decrease as fast as E^{-2} in most cases. They also found, significantly, that various molecules were removed in the sputtering process. These conclusions are supported by the work of Bernhardt et al. (1976) on the sputtering of silver and that of Finn et al. (1976) on sputtering of aluminum oxide. Bernhardt et al. have measured the energy distributions of Ag and Ag_2 sputtered from metallic targets and found that the E^{-2} functional form is approximately correct for both Ag and Ag_2. Finn et al. have observed seven different species emitted during sputtering of aluminum oxide.

One final point concerning this experiment should be emphasized. The technique used measures the energy distribution of individual ^{235}U atoms but cannot make a statement about whether some of those atoms reached the collector as part of molecules or atomic clusters. It is possible that all the collected ^{235}U was sputtered as individual atoms; it is also possible that some could have arrived as U_2, U_3, UO_2 or other complex objects. The spectra of Figures 6 and 8 represent sums over all such possibilities. In the language of the first paragraph of this thesis, one of the discrete variables before the semicolon in $S_i(E,\theta,\cdots;\cdots)$ is an index which labels each molecular species (which contains a ^{235}U atom) that is sputtered. The quantity measured by this technique is what would be obtained by setting i equal to the value appropriate for ^{235}U and summing over this discrete variable.

In conclusion I would like to suggest and comment upon some additional experiments which I feel would be useful. Perhaps the most obvious is to make several additional measurements of energy spectra using both the metal and oxide targets to determine the effect, if any, of changing the bombarding ion, its energy and flux. As discussed previously, it would be of interest to have a measurement of the yield of ^{235}U from a sputtered $^{235}UO_2$ target. An apparatus similar to that used by Gregg (1977) should be used for this experiment and a measurement of the yield of ^{235}U from a metal target should be made simultaneously in order to compare with previous results. In addition, the composition of the $^{235}UO_2$ surface as a function of $^{40}Ar^+$ fluence should be studied using a suitable surface analysis technique.

Rather high priority should be attached to the problem of determining the energy dependence of the sticking fraction. Two independent approaches to this problem should be considered. The first is a measurement similar to that performed by Thompson et al. (1968) in which a second (moving) collector is mounted so that it can intercept material that does not stick to the first. An alternative method is to prepare an analyzed beam of low energy ^{235}U atoms. Two independent methods of doing this should be investigated. In the first, a variant on the present experiment, a pulsed beam and time-of-flight separation could be used. Beam intensity would be a problem in such an experiment. The short pulses and long flight paths necessary for good time-of-flight resolution guarantee this. The availability of a faster motor would enhance the attractiveness of this technique. A second possible method of obtaining a relatively monoenergetic ^{235}U beam might be to magnetically analyze the charged portion

of the sputtered beam (assuming that there is one). If such a separation technique worked, it would also be possible, using track detectors, to measure the fraction of sputtered material that was charged and possibly its momentum distribution as well.

Another possible experiment (and one to which I, as a matter of personal taste, would assign a high priority) is an attempt to observe nonlinear effects in energy spectra. Andersen and Bay (1974) have observed that sputtering yields per incident atom are different for atoms and diatomic molecules of the same velocity. In addition, they have suggested that bombardment by molecules will lead to an increase in the amount of sputtered material at low energy relative to the amount produced by bombardment with atoms. Their data seem to indicate that beams of Cl and Cl_2 will produce a small effect, although it would be better to use beams of elements with even greater atomic number.

Appendix A - Solution of the Equation for p(E,t)

It was stated in the theory section that equation (9) could be solved rigorously for the cross-section given by equation (12). If T is the maximum energy of particles in the collision cascade, then the kernel K(E',E) may be written

$$K(E',E) = \frac{2}{E'} H(E'-E) \quad . \tag{A1}$$

Equation (9) then becomes

$$\frac{\partial p(E,t)}{\partial t} + k\sqrt{E}\, p(E,t) = \phi(E,t) + 2k \int_0^\infty p(E',t)\, H(E'-E)H(T-E')\frac{dE'}{\sqrt{E'}} \quad . \tag{A2}$$

Now denote the Laplace transform of p(E,t) by $\bar{p}(E,s)$ where

$$\bar{p}(E,s) = \int_0^\infty e^{-st}\, p(E,t)\, dt \tag{A3}$$

and define

$$p(E,0) = p(E,t=0) \quad .$$

Applying the Laplace transform to equation (A2) gives

$$(s + k\sqrt{E})\ \bar{p}(E,s) = p(E,0) + \bar{\phi}(E,s) + 2k \int_0^\infty \bar{p}(E',s)H(E'-E)\ H(T-E')\ \frac{dE'}{\sqrt{E'}} \quad . \tag{A4}$$

Differentiate this with respect to E and obtain

$$(s + k\sqrt{E})\ \frac{\partial \bar{p}(E,s)}{\partial E} + \frac{1}{2}\ kE^{-1/2}\ \bar{p}(E,s) = \frac{\partial p(E,0)}{\partial E} + \frac{\partial \bar{\phi}(E,s)}{\partial E}$$

$$- 2k \int_0^{\infty} \bar{p}(E',s)\ \delta(E'-E)\ H(T-E')\ \frac{dE'}{\sqrt{E'}} \quad . \qquad \text{(A5)}$$

Noting the Dirac delta function in the integral, one obtains in the region $E < T$,

$$(s + k\sqrt{E})\ \frac{\partial \bar{p}(E,s)}{\partial E} + \frac{5}{2}\ kE^{-1/2}\ \bar{p}(E,s) = \frac{\partial}{\partial E}\ [p(E,0) + \bar{\phi}(E,s)]$$

or

$$\frac{\partial}{\partial E}\ [(s + k\sqrt{E})^5\ \bar{p}(E,s)] = (s + k\sqrt{E})^4\ \frac{\partial}{\partial E}[p(E,0) + \bar{\phi}(E,s)] \quad . \qquad \text{(A6)}$$

Integrating with respect to E gives

$$(s + k\sqrt{E})^5\ \bar{p}(E,s) = (s + k\sqrt{E})^4\ [p(E,0) + \bar{\phi}(E,s)]$$

$$-2k \int_0^{E} [p(E',0) + \bar{\phi}(E',s)](s + k\sqrt{E'})^3\ \frac{dE'}{\sqrt{E'}} + C(s) \qquad \text{(A7)}$$

where $C(s)$ is an integration constant which may, of course, depend upon s. The right side of equation (A6) has been integrated by parts to give equation (A7).

Rearranging gives

$$\bar{p}(E,s) = \frac{p(E,0) + \bar{\phi}(E,s)}{s + k\sqrt{E}} + \left(\frac{1}{s + k\sqrt{E}}\right)^5 \left[C(s) - 2k \int_0^{E} [p(E',0) \right.$$

$$\left. + \bar{\phi}(E',s)]\ (s + k\sqrt{E'})^3\ \frac{dE'}{\sqrt{E'}} \right] \quad . \qquad \text{(A8)}$$

To find the value of C(s), note (for example from equation (A4)) that $\lim_{E\to T} \bar{p}(E,s) = \frac{p(T,0) + \bar{\phi}(T,s)}{s + k\sqrt{T}}$. Then from (A8)

$$C(s) = 2k \int_0^T [p(E',0) + \bar{\phi}(E',s)] (s + k\sqrt{E'})^3 \frac{dE'}{\sqrt{E'}} \quad . \qquad (A9)$$

Putting this in equation (A8) gives finally

$$\bar{p}(E,s) = \frac{p(E,0) + \bar{\phi}(E,s)}{s + k\sqrt{E}} + 2k \int_E^T [p(E',0) + \bar{\phi}(E',s)] \frac{(s + k\sqrt{E'})^3}{(s + K\sqrt{E})^5} \frac{dE'}{\sqrt{E'}} \quad . \qquad (A10)$$

To obtain the solution to equation (9) one needs only to put in assumptions about p(E,0) and $\phi(E,t)$ and invert the Laplace transform. (As in the text, $\bar{p}(E,s)$ is identically zero for $E > T$.)

Consider the case solved in the text. There

$$p(E,0) = 0 \qquad \text{and} \qquad \phi(E,t) = \phi(E) \qquad (A11)$$

The latter assumption implies that $\bar{\phi}(E,s)$ is $s^{-1}\phi(E)$. Equation (A10) becomes, after a little algebra,

$$\bar{p}(E,s) = \frac{\phi(E)}{k\sqrt{E}} \left[\frac{1}{s} + \frac{1}{s + k\sqrt{E}}\right] + 2k \int_E^T \frac{dE'}{\sqrt{E'}} \phi(E')(s + k\sqrt{E'})^3$$

$$\times \left[\frac{1}{k^5 E^{5/2} s} + \text{terms with powers of } \frac{1}{s + k\sqrt{E}}\right] .$$

When carrying out the Laplace inversion integral, one finds that the terms which contain a factor 1/s are time independent, whereas ones with powers of $(s + k\sqrt{E})^{-1}$ have factors like $e^{-k\sqrt{E}\,t}$. If one is interested

in the steady state, terms containing factors of $(s + k\sqrt{E})^{-1}$ may be ignored. The result is

$$\bar{p}(E,s) = \frac{\phi(E)}{k\sqrt{E}\ s} + \frac{2}{k^4 E^{5/2}} \int_E^T \phi(E') \frac{(s + k\sqrt{E'})^3}{s} \frac{dE'}{\sqrt{E'}} \quad . \tag{A12}$$

This may be inverted to give

$$p(E,t) \rightarrow p(E) = \frac{\phi(E)}{k\sqrt{E}} + \frac{2}{kE^{5/2}} \int_E^T E'\ \phi(E')\ dE'$$

which is precisely the result obtained in the text (equation (19)).

Another interesting result may be obtained from equation (A10) by assuming that

$$\phi(E,t) = 0 \qquad \text{and} \qquad p(E,0) = \delta(E-E_0) \quad , \tag{A13}$$

where the δ is a Dirac delta function and E_0 is less than T. In this case p(E,t) should describe the evolution of an average collision cascade which begins with a single atom moving with energy E_0.

Inserting the expressions (A13) into equation (A10) gives

$$\bar{p}(E,s) = \frac{\delta(E-E_0)}{s + k\sqrt{E}} + 2k \int_E^T \delta(E-E_0) \frac{(s + k\sqrt{E'})^3}{(s + k\sqrt{E})^5} \frac{dE'}{\sqrt{E'}} \quad . \tag{A14}$$

Consider the two regions $E > E_0$ and $E \leq E_0$ separately. The first of these is trivial.

$$\bar{p}(E,s) = 0 \rightarrow p(E,t) = 0 \qquad \text{for } E > E_0 \quad . \tag{A15}$$

For the more interesting case,

$$\bar{p}(E,s) = \frac{\delta(E-E_0)}{s + k\sqrt{E}} + \frac{2k}{\sqrt{E_0}} \frac{(s + k\sqrt{E_0})^3}{(s + k\sqrt{E})^5} \quad . \tag{A16}$$

A straightforward application of the Laplace inversion integral gives

$$p(E,t) = e^{-k\sqrt{E}\,t}\,\delta(E-E_0) + \frac{2kt}{\sqrt{E_0}} e^{-k\sqrt{E}\,t} \left[1 + \frac{3}{2} k(\sqrt{E_0} - \sqrt{E})t \right.$$

$$\left. + \frac{1}{2} k^2(\sqrt{E_0} - \sqrt{E})^2 t^2 + \frac{1}{24} k^3(\sqrt{E_0}-\sqrt{E})^3 t^3\right]. \tag{A17}$$

Let the dimensionless parameter τ be defined by the equation $t = \tau/(k\sqrt{E_0})$. (For this experiment, the time unit $1/(k\sqrt{E_0})$ is about 10^{-15} seconds.)

Then

$$p(E,\tau) = e^{-\tau\sqrt{E/E_0}}\,\delta(E-E_0) + \frac{2\tau}{E_0} e^{-\tau\sqrt{E/E_0}} \left[1 + \frac{3\tau}{2}(1 - \sqrt{E/E_0}) \right.$$

$$\left. + \frac{\tau^2}{2} (1 - \sqrt{E/E_0})^2 + \frac{\tau^3}{24} (1 + \sqrt{E/E_0})^3\right] \quad . \tag{A18}$$

The functions $p(E,\tau)$ are plotted for $E_0 = 1$ and $\tau = 0.01$, 1, 10, 40, and 100 in Figure 10. Note that for $\tau = 0.01$ $p(E,\tau)$ is almost a constant. This is the result to be expected if approximately one hard-sphere collision had occurred. In Figure 11 is plotted the total number of moving particles as a function of τ. This is, of course, just the integral of $p(E,\tau)$ over all E. The function $Ep(E,\tau)$ gives the amount of energy that is being carried by particles whose energy is in the range E to E+dE. This function is plotted for several values of τ in Figure 12. Again, E_0 is set equal to 1. A final quantity of interest is the fraction of

the total energy that is carried by particles whose energy is greater than some given energy E. Denote this quantity by $f(E/E_0)$. Then

$$f(\frac{E}{E_0}) = \frac{1}{E_0} \int_{E}^{E_0} E' \, p(E',\tau) \, dE' \quad . \tag{A19}$$

$f(E/E_0)$, which is independent of E_0, is plotted for several values of τ in Figure 13.

Appendix B - A Digital Current Integrator

As indicated in Figure 2, one of the elements of the total system used to make the energy spectrum measurements described in this thesis was a current integrator. Its function was to integrate the beam current incident on the uranium and UO_2 targets. In its design, maximum use was made of currently available monolythic integrated circuits and discrete component function modules. This resulted in a very simple apparatus for which the accuracy and cost compare favorably with commercially available instruments that perform a similar function. Two devices, in particular, made this accuracy and simplicity possible. The first was a modular voltage to frequency converter (VFC), the AD454K, manufactured by Analog Devices, Inc., Norwood Mass. This device produced a train of logic pulses whose frequency was 1 kHz per input volt. The guaranteed maximum nonlinearity of the output was $\sim$0.015%. The second device was a film resistor manufactured by Caddock Electronics, Inc., Riverside, CA, that had a total resistance of 10 MΩ (nominal tolerance ±0.25%) and was tapped to provide voltage divisions in decade steps from 0.1 to 0.0001 with ratio errors of less than 0.05%.

Figure 14 is a functional schematic of the integrator. The operational amplifiers indicated, the AD52K and OP-07EY, were chosen for their high open loop gains and especially for their superior offset stability. The AD52K with the decade resistor chain in its feedback loop serves as an input current-to-voltage converter. For negative input currents, the AD52K output voltage may be fed directly into the VFC. For positive input currents the AD52K output is negative and an inversion is necessary before the signal can be applied to the VFC. This is

provided by the OP-07EY which is wired as a unity gain inverting amplifier.

The output pulses from the VFC are fed into a NAND gate which provides for external gating of the output pulses and buffers the VFC. Three additional NAND gates with their outputs wired in parallel serve as a line driver. This arrangement is capable of driving a 50Ω terminated cable. All four NAND gates used are in one package, the 74H00.

Because the film resistors in the feedback loop of the AD52K amplifier have highly accurate resistance ratios, a single adjustment at the input of the VFC calibrates all ranges of the instrument at once. The only other adjustments that are necessary are offset voltage nulling of the VFC and the amplifiers. The input impedance of the integrator (2Ω) is determined completely by the resistance of the 1/4A fuse that serves as protection against catastrophic input overloads. (The maximum current that can be reliably digitized is about ±1.2 mA.) The estimated maximum error of the instrument is 0.5% for currents in the range 1 nA to 1.2 mA. For smaller currents offset voltage errors become important and degrade accuracy.

REFERENCES

Andersen, H. H. and Bay, H. L., 1974, J. Appl. Phys. 45, 953.

Andersen, N. and Sigmund, P., 1974, Matt. Fys. Medd. Dan. Vid. Selsk. 39, 3.

Arifov, U. A., Gruich, D. D., Ermakov, G. E., Parilis, E. S., Turayev, N. Y. and Umarov, F. F., 1973, Rad. Eff. 19, 219.

Bernhardt, F., Oechsner, H. and Stumpe, E., 1976, Nucl. Instr. Meth. 132, 329.

Beuscher, H. and Kopitzki, K., 1965, Z. Physik 184, 382.

Chapman, G. E., Farmery, B. W., Thompson, M. W. and Wilson, I. H., 1972, Rad. Eff. 13, 121.

Farmery, B. W. and Thompson, M. W., 1968, Phil. Mag. 18, 415.

Finn, P. A., Gruen, D. M. and Page, D. L., 1976, in M. Kaminsky (ed.) Radiation Effects on Solid Surfaces (American Chemical Society, Washington), p. 30.

Gregg, R., 1977, Ph.D. Thesis, California Institute of Technology.

Gregg, R., Switkowski, Z. E. and Tombrello, T. A., 1977, Nucl. Instr. Meth. 144, 613.

Gregg, R. and Tombrello, T. A., 1977, Rad. Eff., in press.

Griffith, J. E., Weller, R. A. and Tombrello, T. A., 1978, Bull. Am. Phys. Soc. 23, 32.

Gschneidner, Jr., K. A., 1964, Solid State Phys. 16, 275.

Haff, P. K., Switkowski, Z. E., Burnett, D. S. and Tombrello, T. A., 1977. Proc. Lunar Sci. Conf. 8th (Pergamon Press, New York), p. 3807.

Hulpke, E. and Schlier, C. H., 1967, Z. Physik 207, 294.

Kelley, R. and Lam, N. Q., 1973, Rad. Eff. 19, 39.

Können, G. P., Grosser, J., Haring, A., DeVries, A. E. and Kistemaker, J., 1974, Rad. Eff. 21, 171.

Kostin, M. D., 1965, J. Appl. Phys. 36, 850.

Lindhard, J., Scharff, M. and Schiøtt, H. E., 1963, Mat. Fys. Medd. Dan. Vid. Selsk. 33, 14.

McCracken, G. M., 1975, Rep. Prog. Phys. 38, 24.

Mathews, J. and Walker, R. L., 1970, Mathematical Methods of Physics (W. A. Benjamin, Inc., New York), p. 375.

Miyagawa, S., 1973, J. Appl. Phys. 44, 5617.

Oechsner, H. and Reichert, L., 1966, Phys. Lett. 23, 90.

Politiek, J. and Kistemaker, J., 1969, Rad. Eff. 2, 129.

Reid, I., Farmery, B. W. and Thompson, M. W., 1976, Nucl. Instr. Meth. 132, 317.

Robinson, M. T., 1965, Phil. Mag. 12, 145.

Robinson, M. T., 1970, in D. W. Palmer et al. (eds.) Atomic Collision Phenomena in Solids (North Holland, Amsterdam), p. 66.

Roth, A., 1976, Vacuum Technology (North Holland, Amsterdam), p. 337.

Sigmund, P., 1972, Rev. Roum. Phys. 17, 823.
1972a, Rev. Roum. Phys. 17, 969.
1972b, Rev. Roum. Phys. 17, 1079.

Stuart, R. V. and Wehner, G. K., 1964, J. Appl. Phys. 35, 1819.

Stuart, R. V., Wehner, G. K. and Anderson, G. S., 1969, J. Appl. Phys. 40, 803.

Thompson, M. W., Farmery, B. W. and Newson, P. A., 1968, Phil. Mag. 18, 361.

Thompson, M. W., 1968, Phil. Mag. 18, 377.

Williams, M.M.R., 1976, Phil. Mag. 34, 669.

Figure 1

A diagram of the complete system used in the experiment. At the lower right is an expanded view of the spectrometer chamber which shows, in particular, the motor and disk. An unmounted disk is depicted at the upper left (see Section III.A).

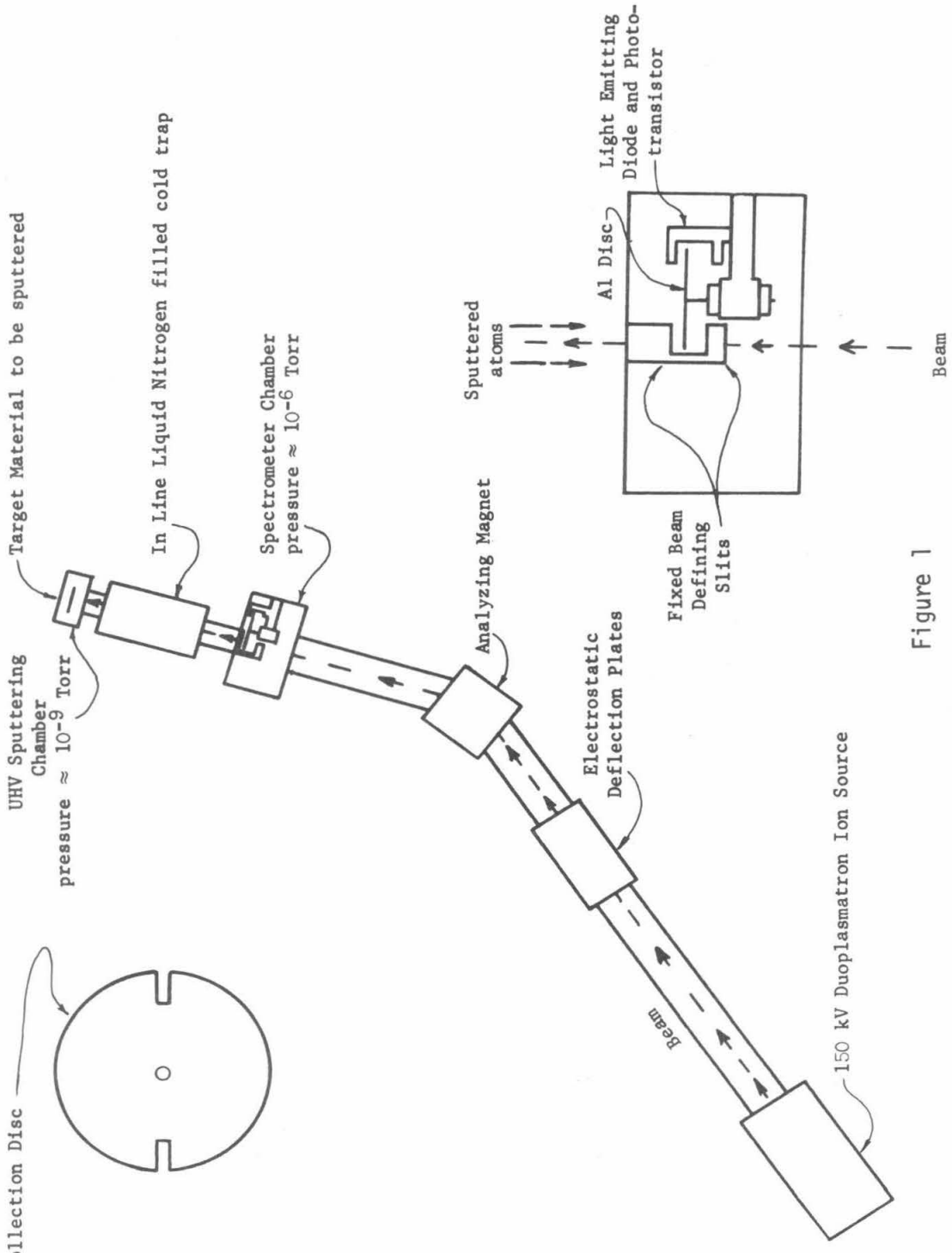
Collection Disc
UHV Sputtering Chamber pressure ≈ 10-9 Torr
Target Material to be sputtered
In Line Liquid Nitrogen filled cold trap
Spectrometer Chamber pressure ≈ 10-6 Torr
Analyzing Magnet
Sputtered atoms
Al Disc
Light Emitting Diode and Photo-transistor
Fixed Beam Defining Slits
Electrostatic Deflection Plates
Beam
150 kV Duoplasmatron Ion Source
Beam

Figure 1

Figure 2

A functional schematic of the time-of-flight spectrometer electrical system. For clarity, the motor power source is not shown (see Section III.A).

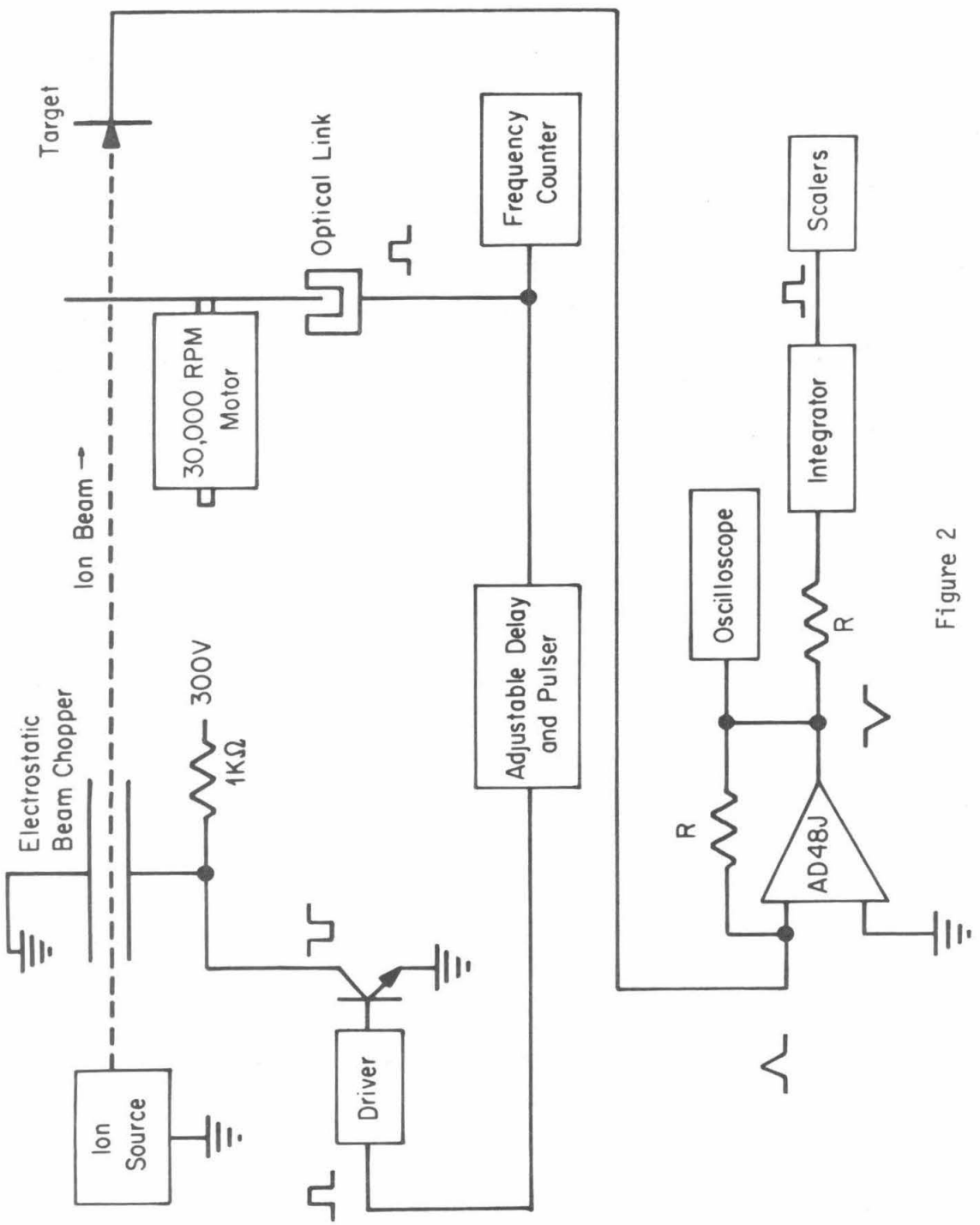
Target
Optical Link
Frequency Counter
30,000 RPM Motor
Ion Beam
Electrostatic Beam Chopper
300V
1KΩ
Adjustable Delay and Pulser
Ion Source
Driver
Oscilloscope
Integrator
Scalers
R
R
AD48J

Figure 2

Figure 3

An aluminum collector wheel. The dashed lines on the wheel at the left indicate the lines along which the wheel was cut prior to neutron irradiation. At the right is shown a typical disk segment. The location of the area covered with ^{235}U is indicated (see Section IV.B).

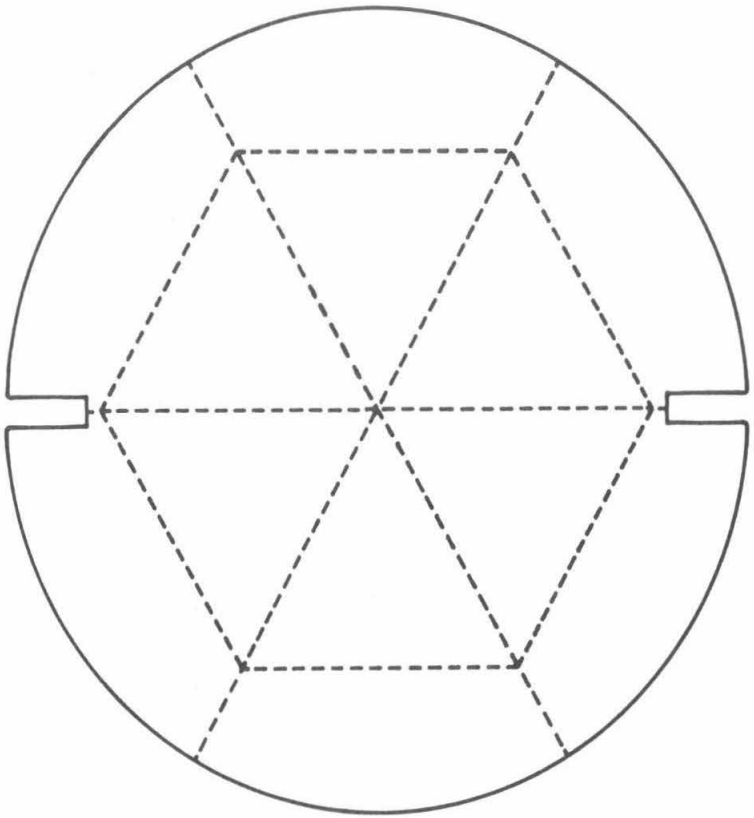

Reference Radius

Collector Disk

^{235}U Covered Region

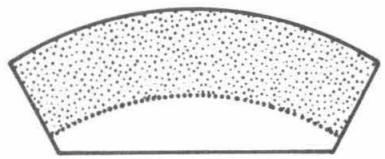

Typical Disk Segment After Cutting

Figure 3

Figure 4

The functions $[\gamma(z,13.9) + \varepsilon(z,13.9)]$ (smooth curve) and $\lambda(z,13.9)$ (crosses), that describe the predicted result of measuring a spectrum $E/(E+5.4)^3$ with the instrument used in this experiment, and an ideal spectrometer, respectively. The excellent agreement indicates that the systematic error introduced by the measurement process is small (see Section V.A).

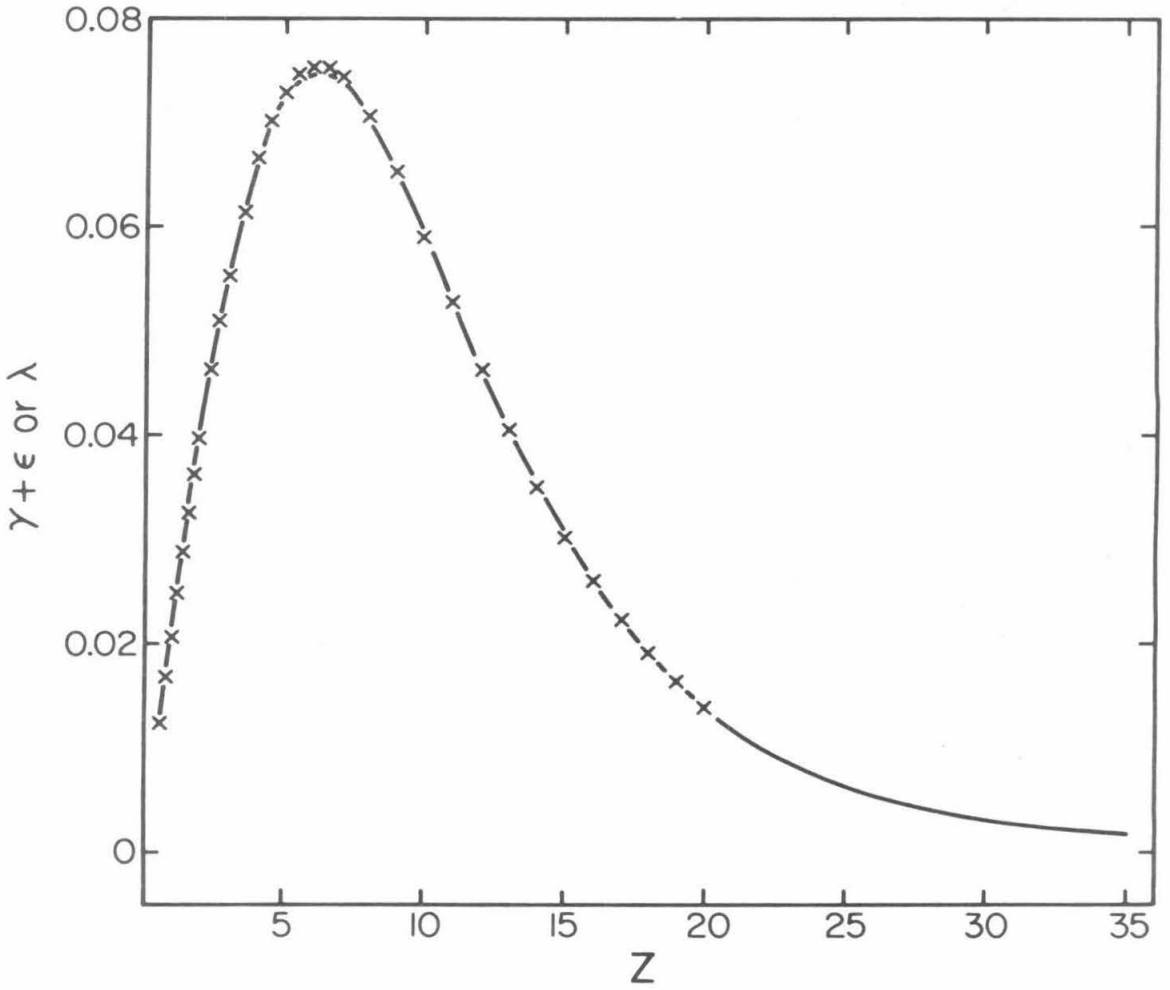

Figure 4

Figure 5

The arrival time spectrum for ^{235}U atoms sputtered from a ^{235}U metal target. The track density, N(z), (= $\sigma\Phi$ p(z)) in units of cm^{-2} is plotted as a function of position, z, on the collector wheel. Distance, z, is measured in units of the spectrometer slit widths (0.447 cm). The representative error bars shown are statistical (see Section V.B).

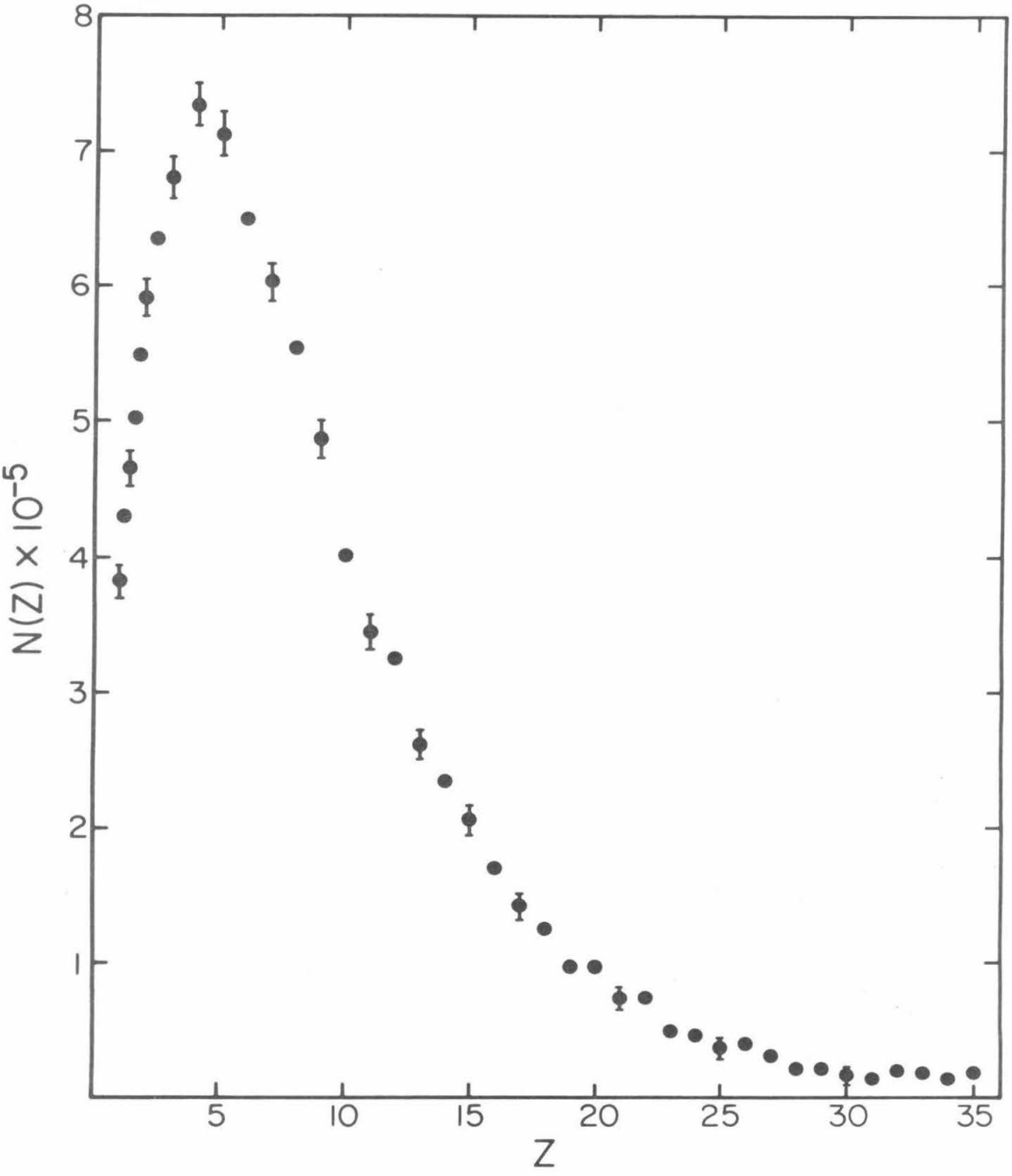

Figure 5

Figure 6

The energy spectrum, S(E), of ^{235}U sputtered from a uranium metal target. The spectrum (data points with statistical error bars) has been inferred from the data of Figure 5 by using equation (56). The vertical scale is arbitrary. The smooth curve is an empirical fit to the data (see equation (58)). The dashed curve is a Thompson spectrum (Thompson 1968) of the form $6.5E/(E+5.4)^3$. Both curves and the data have been normalized to agree near the peak (see Sections V.A and V.B).

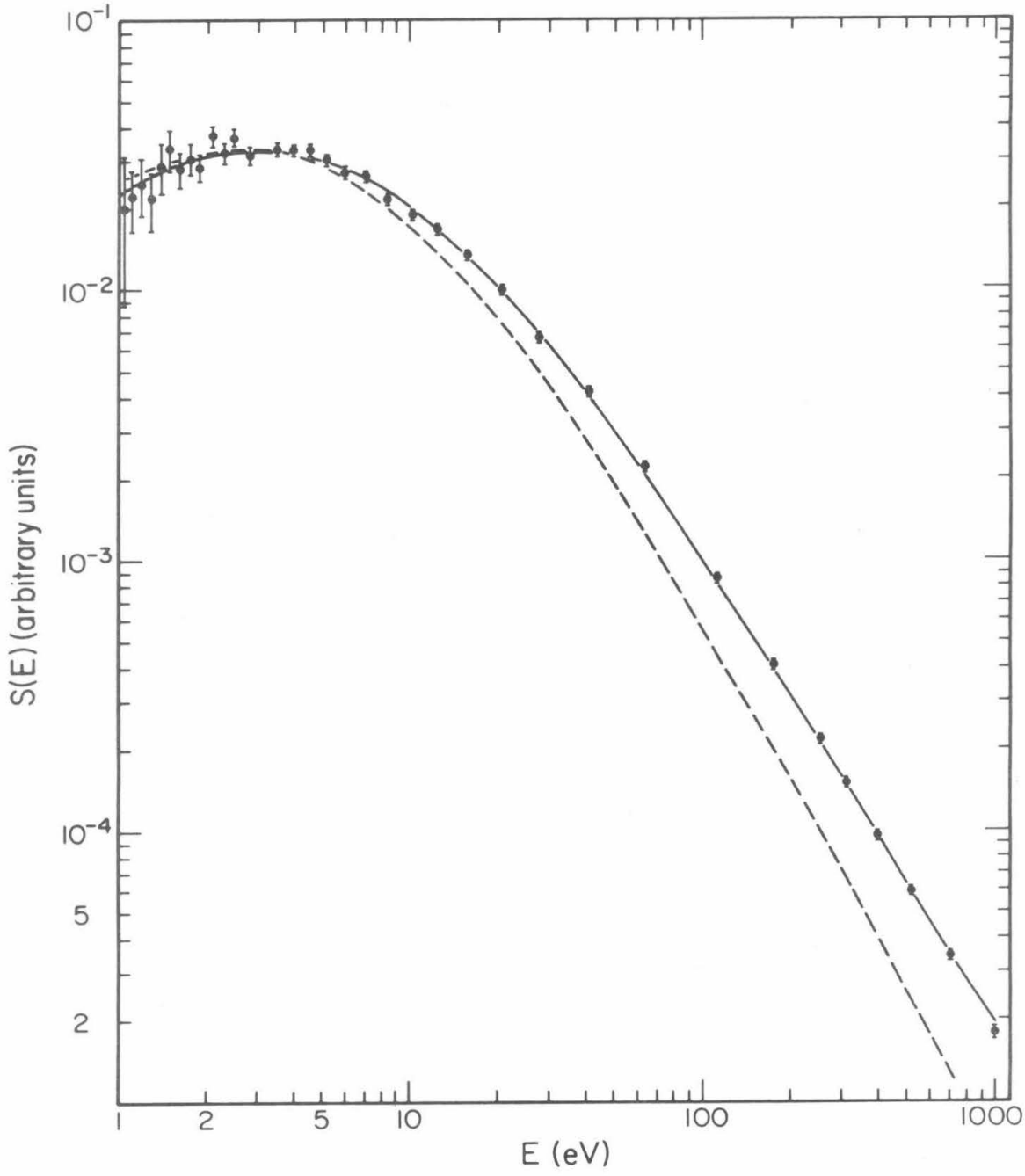

Figure 6

Figure 7

The arrival time spectrum of ^{235}U atoms sputtered from a $^{235}UO_2$ target. The track density, N(z), in units of cm^{-2} is plotted as a function of position, z, on the collector. Note the similarity to Figure 5. The representative error bars shown are statistical (see Section V.B).

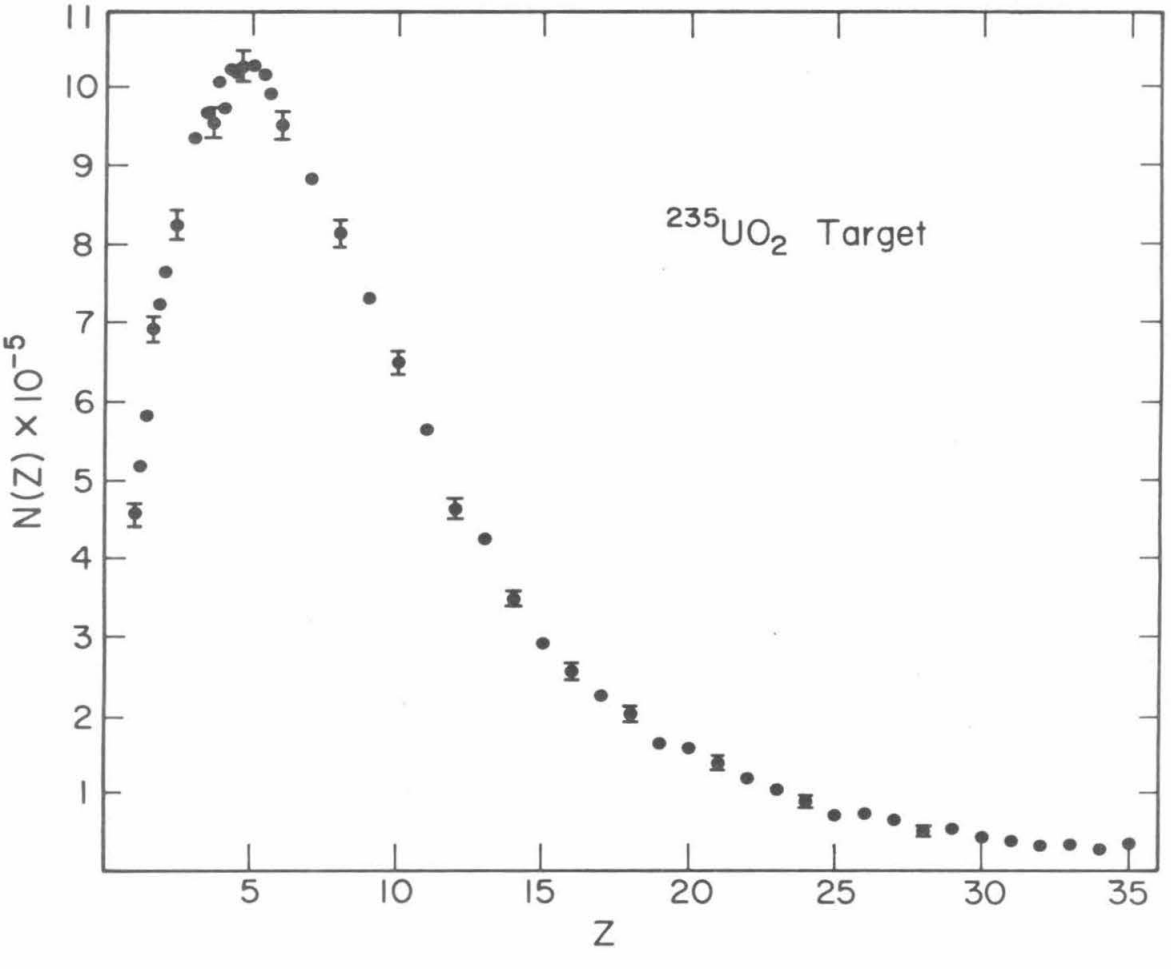

Figure 7

Figure 8

The energy spectrum, S(E), of ^{235}U sputtered from a $^{235}UO_2$ target. The spectrum (data points) has been inferred from the data of Figure 7 by using equation (56). The vertical scale is arbitrary. For energies greater than about 100 eV the spectrum decreases as $E^{-1.86}$ (see Section V.B).

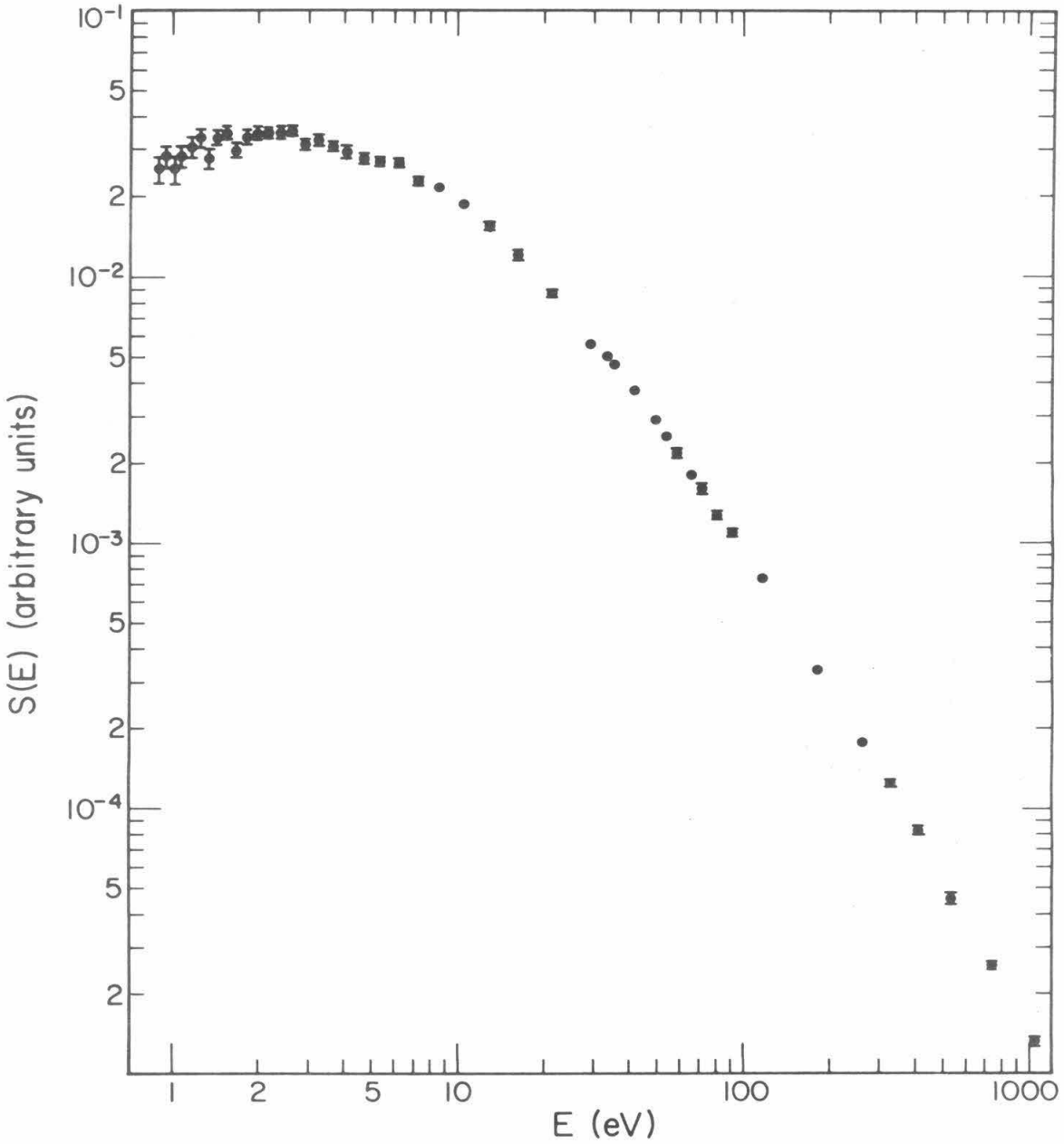
S(E) (arbitrary units)
E (eV)
10⁻¹
5
2
10⁻²
5
2
10⁻³
5
2
10⁻⁴
5
2
1
2
5
10
100
1000

Figure 8

Figure 9

The experimental energy spectra of Figures 6 and 8 have been plotted together for comparison. The vertical scales have been normalized. The closed circles are from Figure 8, while the open triangles are from Figure 6 (see Section V.B).

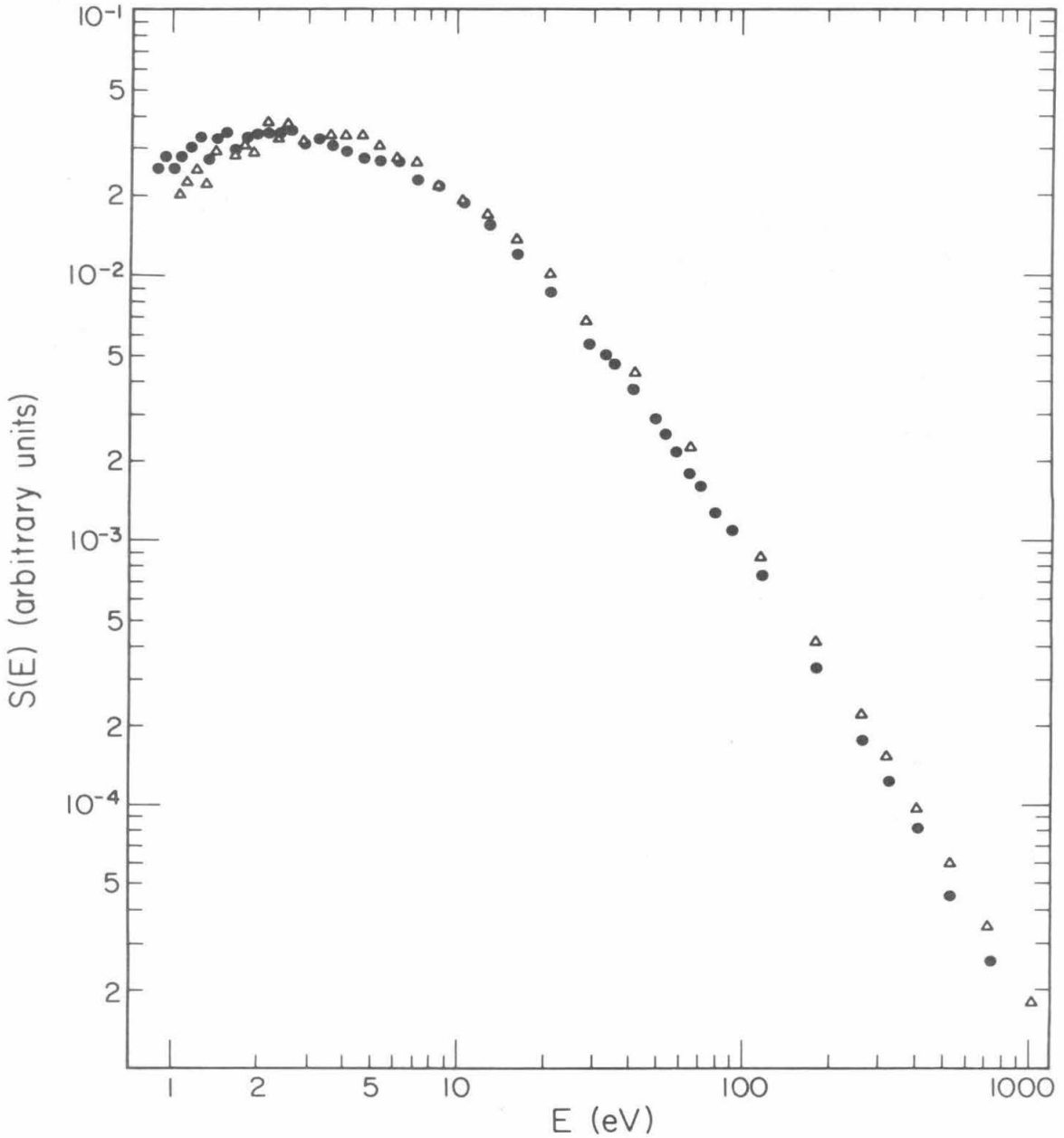
S(E) (arbitrary units)
E (eV)
10⁻¹
5
2
10⁻²
5
2
10⁻³
5
2
10⁻⁴
5
2
1
2
5
10
100
1000

Figure 9

Figure 10

The energy distributions, $p(E,\tau)$, of atoms in a collision cascade at times τ = 0.01, 1, 10, 40, and 100. The cascade is assumed to have begun at τ = 0 with one particle moving at energy E_0. τ is a dimensionless time parameter (see Appendix A).

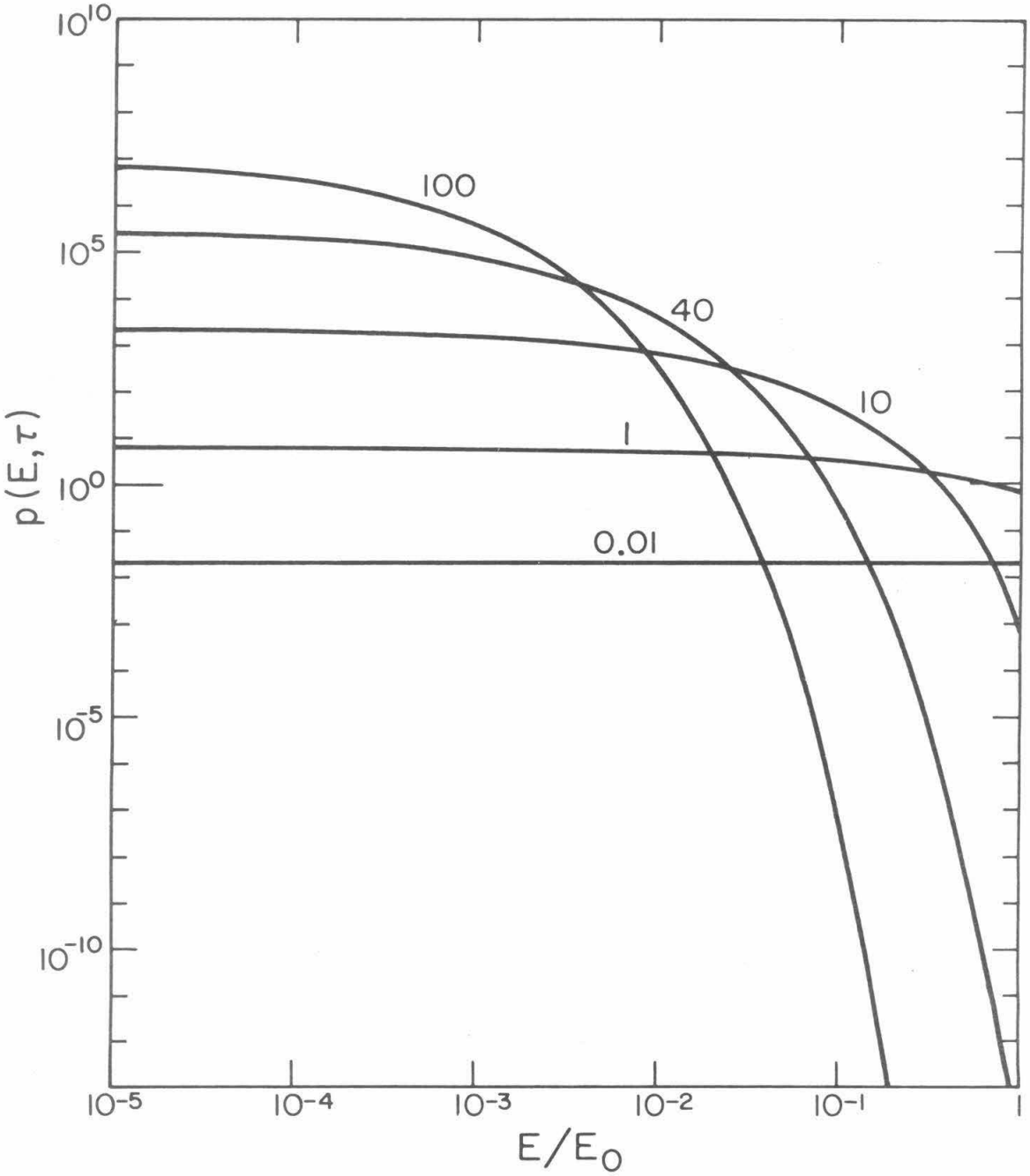
10^{10}
10^{5}
10^{0}
10^{-5}
10^{-10}
$p(E,\tau)$
100
40
10
1
0.01
10^{-5}
10^{-4}
10^{-3}
10^{-2}
10^{-1}
1
E/E_0

Figure 10

Figure 11

The number of atoms moving in a collision cascade, $\int p(E,\tau)dE$, as a function of τ . τ is a dimensionless time parameter (see Appendix A).

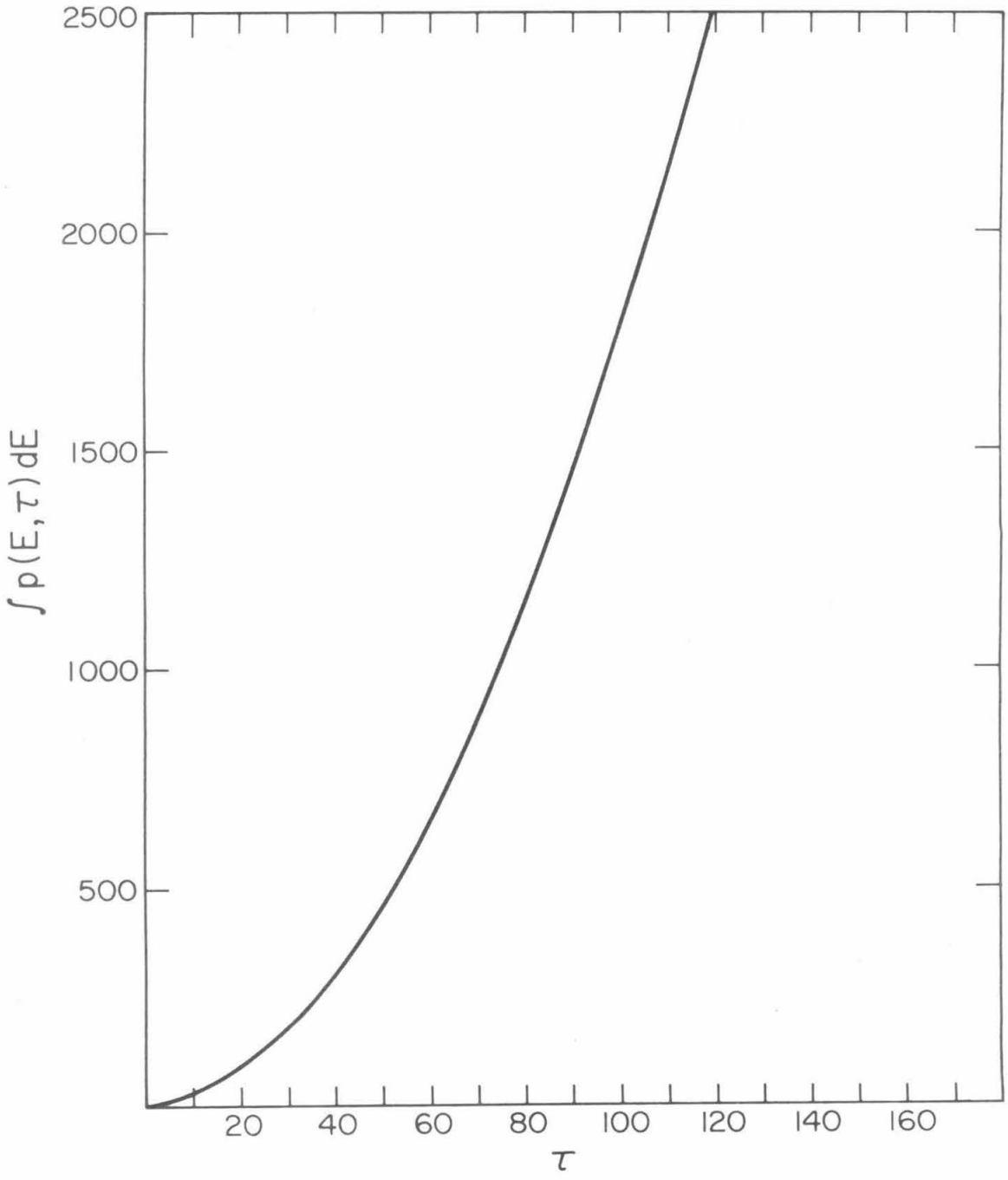
2500
2000
1500
1000
500
$\int p(E,\tau)\,dE$
20
40
60
80
100
120
140
160
τ

Figure 11

Figure 12

The quantity $Ep(E,\tau)$ as a function of E/E_0 for various values of τ (τ = 0.01, 1, 10, 40, 100, and 400). $Ep(E,\tau)dE$ is the portion of the original energy being carried by atoms whose energy is between E and E+dE. In this graph E_0 is taken to be 1. The collision cascade being described is assumed to have begun at time τ = 0 with one atom of energy E_0 moving (see Figure 10 and Appendix A).

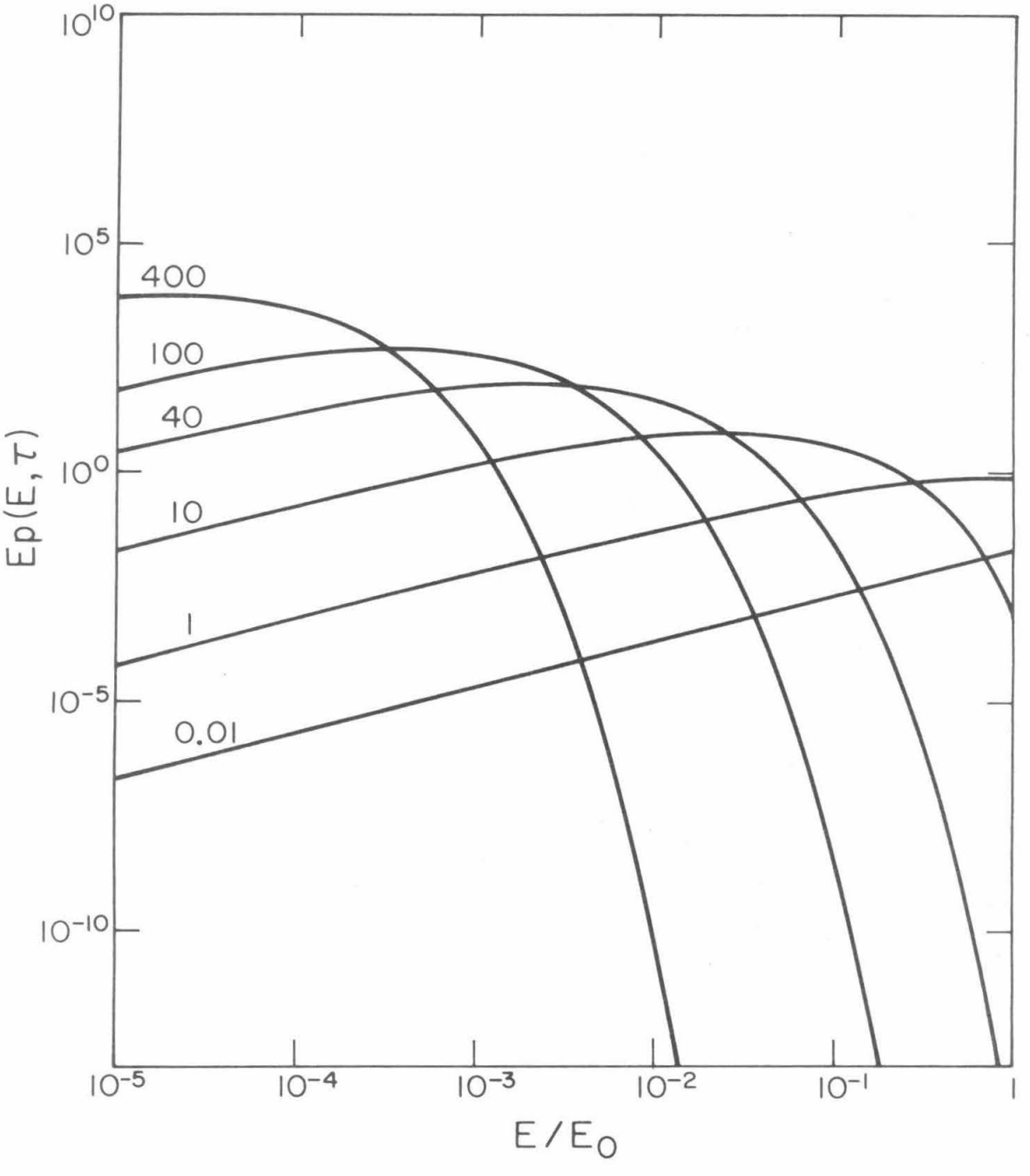
10^{10}
10^{5}
10^{0}
10^{-5}
10^{-10}
400
100
40
10
1
0.01
$Ep(E,\tau)$
10^{-5}
10^{-4}
10^{-3}
10^{-2}
10^{-1}
1
E/E_0

Figure 12

Figure 13

The function $f(E/E_0)$ for several values of τ (τ = 0.01, 1, 10, 40, and 100). The collision cascade being described is assumed to have begun at time $\tau = 0$ with one moving atom of energy E_0. $f(E/E_0)$ gives the fraction of the original energy being carried by particles whose energy is greater than E. As expected, at later times, virtually none of the original energy is being transported by highly energetic individual atoms (see Figure 12 and Appendix A).

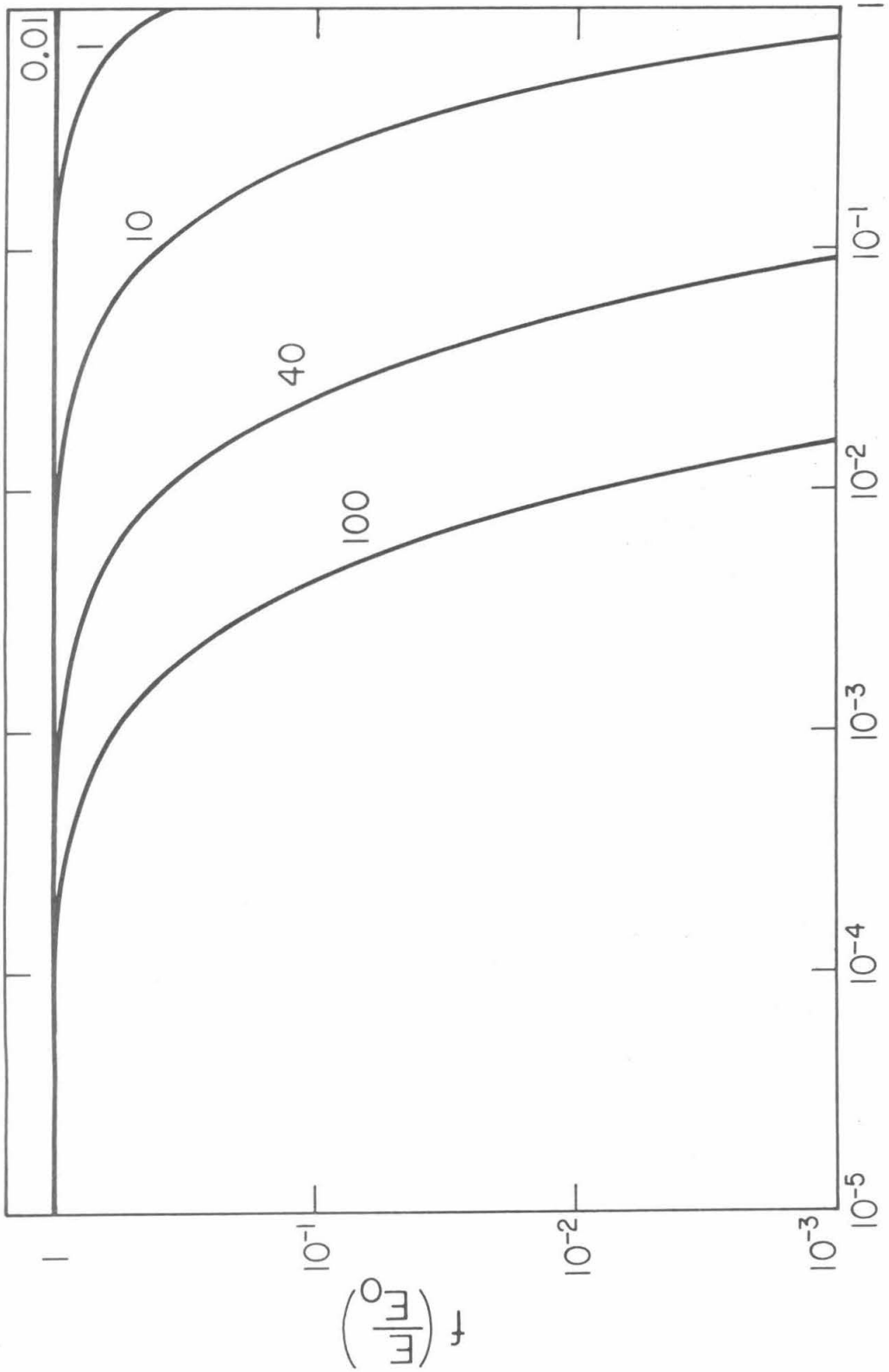
0.01
1
10
40
100
1
10^{-1}
10^{-2}
10^{-3}
10^{-1}
10^{-2}
10^{-3}
10^{-4}
10^{-5}
1
E/E_0
$f\left(\frac{E}{E_0}\right)$

Figure 13

Figure 14

Functional schematic of a digital current integrator for general laboratory use. A description of the circuit is given in Appendix B.

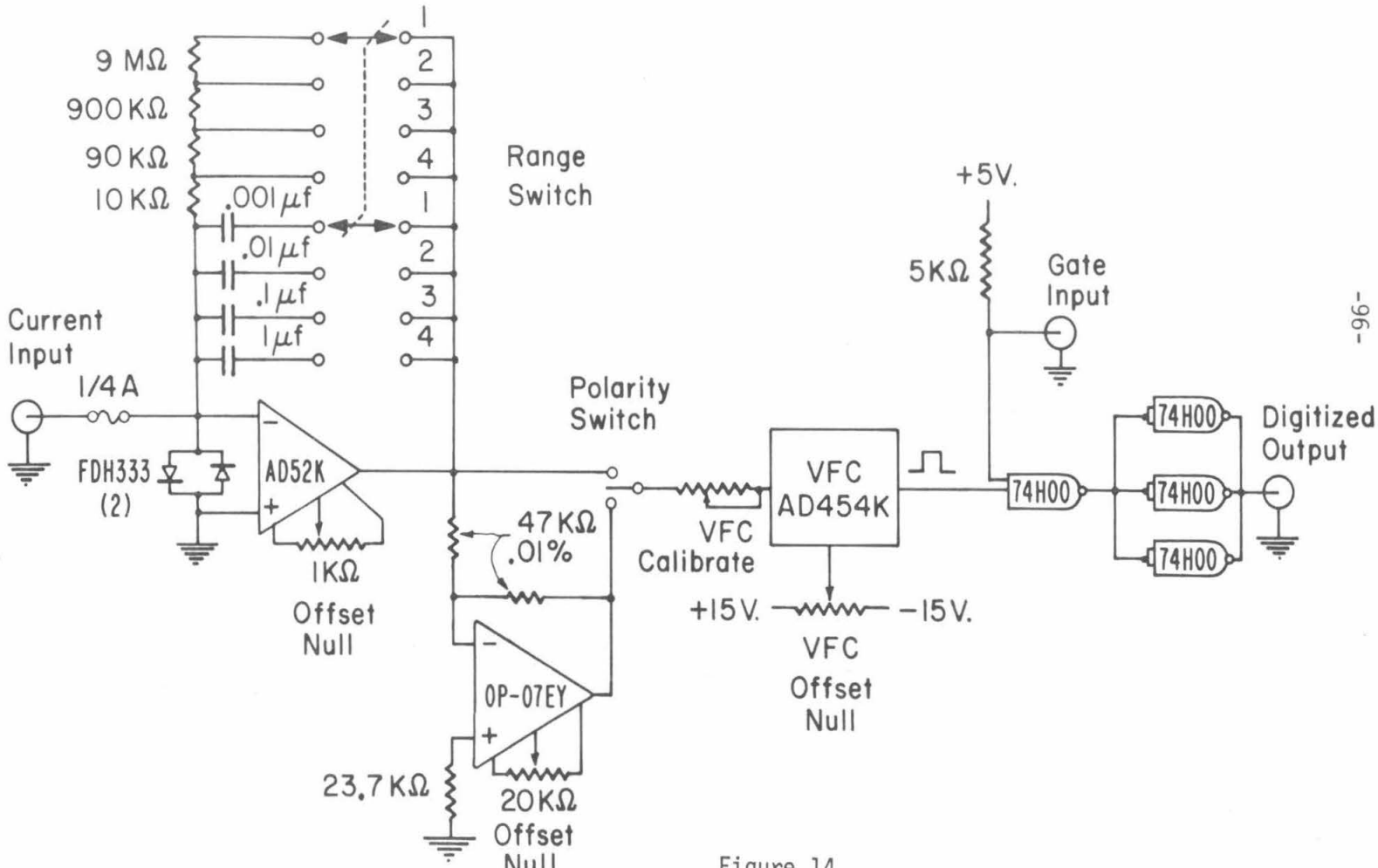
9 MΩ
900 KΩ
90 KΩ
10 KΩ
.001 μf
.01 μf
.1 μf
1 μf
1
2
3
4
Range Switch
Current Input
1/4 A
FDH333 (2)
AD52K
1KΩ
Offset Null
47 KΩ .01%
OP-07EY
23.7 KΩ
20KΩ
Offset Null
Polarity Switch
VFC Calibrate
VFC AD454K
+15V.
−15V.
VFC Offset Null
+5V.
5KΩ
Gate Input
74H00
74H00
74H00
74H00
Digitized Output

Figure 14

Figure 15

The fraction of sputtered particles with energy less than E when the energy distribution is assumed to be given by equation (58). Note that almost all particles fall within the measured energy range of 1 eV to 1 keV. The additional significance of this graph is discussed in Section V.C.

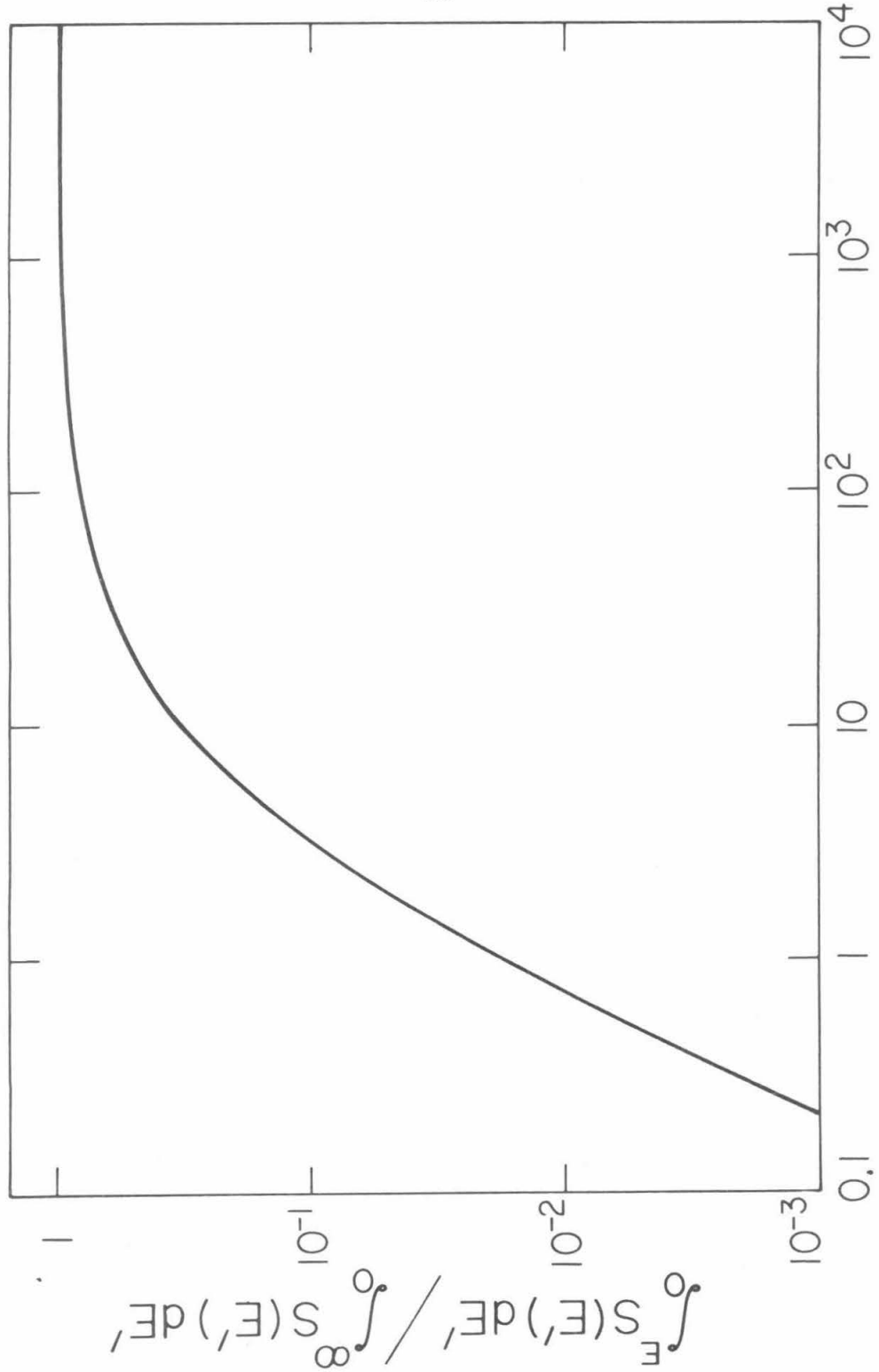

Figure 15